

LIBRARY Michigan State University

This is to certify that the thesis entitled

Measuring the Phase Synchrony of Brain Signals Using Time-Frequency Distributions

presented by

Westley Evans

has been accepted towards fulfillment of the requirements for the

M.S.	degree in	Electrical Engineering
	Strigente	
-,-	Major Profess	or's Signature
	12/01/	2008
	Da	ate

MSU is an Affirmative Action/Equal Opportunity Employer

PLACE IN RETURN BOX to remove this checkout from your record. **TO AVOID FINES** return on or before date due. **MAY BE RECALLED** with earlier due date if requested.

DATE DUE	DATE DUE	DATE DUE
		4 10

5/08 K:/Proj/Acc&Pres/CIRC/DateDue.indd

MEASURING THE PHASE SYNCHRONY OF BRAIN SIGNALS USING TIME-FREQUENCY DISTRIBUTIONS

By

Westley Evans

A THESIS

Submitted to
Michigan State University
in partial fulfillment of the requirements
for the degree of

MASTER OF SCIENCE

Electrical Engineering

2008

ABSTRACT

MEASURING THE PHASE SYNCHRONY OF BRAIN SIGNALS USING TIME-FREQUENCY DISTRIBUTIONS

By

Westley Evans

Quantifying the phase synchrony of brain signals is important for the study of large-scale interactions in the brain. Current methods for computing phase synchrony are limited to amplitude-dependent correlation methods, frequency-domain coherence methods, and wavelet transform methods. However, many of these methods fail to take the time-varying nature of real life signals into account. To address this issue, we propose two measures of phase synchrony based on Cohen's class of time-frequency distributions. The first proposed method measures the phase synchrony between a pair of signals using a time-varying estimate of the phase difference between the two signals. The phase difference estimate is computed using a reduced interference complex time-frequency distribution. The second proposed method measures the phase synchrony among a group of signals by quantifying the frequency locking among the signals using a time-frequency based estimation of the instantaneous frequency. The instantaneous frequency maps of individual signals are combined to obtain the instantaneous frequency histogram as an estimate of the amount of frequency locking across the signals. This analysis is then extended to the estimation of frequency locking across multiple electrodes and multiple trials. Results are shown for both methods using synthetic signal models and electroencephalogram (EEG) data collected from control and schizophrenic subjects.

TABLE OF CONTENTS

LIST O	F TABLES	v
LIST O	F FIGURES	vi
KEY T	O SYMBOLS AND ABBREVIATIONS	ix
СНАРТ	ER 1	
Introdu	ction	1
1.1	Problem Statement	1
1.2	Contributions of Thesis	
1.3	Organization of Thesis	
СНАРТ	'ER 2	
Backgro	ound	4
2.1	Electroencephalogram	4
2.2	• •	5
2.3	Time-Frequency Distributions	6
	2.3.1 Cohen's Class of TFDs and the Wigner Distribution	8
	· · · · · · · · · · · · · · · · · · ·	8
		10
		11
СНАРТ	YER 3	
	e Phase Synchrony	16
3.1		16
3.2	9 ,	19
3.3	,	20
3.4	• •	$\frac{20}{21}$
0.1	3 7	22
	· · ·	$\frac{22}{22}$
	3.4.3 Comparison Between the Wavelet and Rihaczek based Phase	
		23
СНАРТ	ER 4	
Multiva	riate Phase Synchrony	27
4.1		27
4.2	1 3	28
4.3		30
4.4		31
4.5		34
4.6		34

CHAPT	ER 5		
Results			
5.1	Gamma Band Synchrony in Schizophrenic Subjects		
5.2	Bivariate Phase Synchrony in Schizophrenic Subjects		
5.3	Multivariate Phase Synchrony in Schizophrenic Subjects 44		
СНАРТ	CER 6		
Conclus	ions and Future Work		
6.1	Contributions		
6.2	Future Work		
	6.2.1 Multivariate Method Improvements 60		
	6.2.2 Volume Conduction		
	6.2.3 Directional Measures		
	6.2.4 Functional Networks		
BIBLIO	GRAPHY		

LIST OF TABLES

Table 2.1	The frequency bands of an EEG signal	5
Table 5.1	The correlation averages in five different frequency bands for the four most significant centroids of each control subject	57
Table 5.2	The correlation averages in five different frequency bands for the four most significant centroids of each schizophrenic subject	58
Table 5.3	The weighted average of the correlation averages for the four most significant centroids of each control and schizophrenic subject in five different frequency bands. The final row contains the difference between the average control subject's correlation average and the average schizophrenic subject's correlation average	58

LIST OF FIGURES

Figure 2.1	a) The real component of a complex exponential chirp signal that increases in normalized frequency from 0.05 to 0.35, b) the magnitude of the FT for the chirp signal, and c) the Wigner TFD of the same chirp signal	12
Figure 2.2	a) The non-uniform time-frequency resolution of the wavelet transform and b) the uniform time-frequency resolution of Cohen's class of TFDs	13
Figure 2.3	a) Wigner distribution and b) Choi-Williams distribution for the sum of two Gabor logons	14
Figure 2.4	The ambiguity domain for the sum of two Gabor logons	15
Figure 3.1	a) Magnitude of Rihaczek distribution and b) Magnitude of reduced interference Rihaczek distribution	24
Figure 3.2	a) Real component of the two complex exponentials and b) Comparison of the theoretical and estimated time-varying phase difference of the two complex exponentials	25
Figure 3.3	Average PLV for two chirps with a constant phase difference: a) wavelet distribution, b) Rihaczek distribution	26
Figure 4.1	Example of estimating IF on a multicomponent signal. Black indicates the expected IF, and gray indicates the estimated IF	31
Figure 4.2	Synthetic signals (a) $x_1(t)$ and (b) $x_2(t)$	35
Figure 4.3	The IFH of a pair of synthetic signals with common IF from 0 to 1 seconds and from 2 to 3 seconds	35
Figure 5.1	Average PLV between electrode pairs in the γ band of the P300 time window for the four control subjects. The diagonal of the figure, which is the PLV of an electrode with itself, is set to zero rather than one to improve scaling	38
Figure 5.2	Average PLV between electrode pairs in the γ band of the P300 time window for the four schizophrenic subjects. The diagonal of the figure, which is the PLV of an electrode with itself, is set to zero rather than one to improve scaling	39
Figure 5.3	The Average PLV difference between control and schizophrenic subjects	40

Figure 5.4	Average PLV with respect to electrode Fz for the four control subjects	41
Figure 5.5	Average PLV with respect to electrode Fz for the four schizophrenic subjects	42
Figure 5.6	Difference of the average PLV with respect to electrode Fz between the control and schizophrenic subjects	43
Figure 5.7	Topographic map of the average PLV with respect to Fz for four control subjects.	44
Figure 5.8	Topographic map of the average PLV with respect to Fz for four schizophrenic subjects.	45
Figure 5.9	Topographic map of the difference of the average PLV with respect to Fz between control and schizophrenic subjects	46
Figure 5.10	The four most significant cluster centroids of control subject 1. The number of IFHs belonging to each cluster: (a) 15, (b) 14, (c) 3, (d) 3	49
Figure 5.11	The four most significant cluster centroids of control subject 2. The number of IFHs belonging to each cluster: (a) 12, (b) 6, (c) 5, (d) 4	50
Figure 5.12	The four most significant cluster centroids of control subject 3. The number of IFHs belonging to each cluster: (a) 21, (b) 6, (c) 5, (d) 4	51
Figure 5.13	The four most significant cluster centroids of control subject 4. The number of IFHs belonging to each cluster: (a) 60, (b) 7, (c) 3, (d) 3	52
Figure 5.14	The four most significant cluster centroids of schizophrenic subject 1. The number of IFHs belonging to each cluster: (a) 27, (b) 21, (c) 5, (d) 3	53
Figure 5.15	The four most significant cluster centroids of schizophrenic subject 2. The number of IFHs belonging to each cluster: (a) 32, (b) 8, (c) 2, (d) 1	54
Figure 5.16	The four most significant cluster centroids of schizophrenic subject 3. The number of IFHs belonging to each cluster: (a) 5, (b) 3, (c) 3, (d) 2	55

Figure 5.17	The four most significant cluster centroids of schizophrenic sub-	
	ject 4. The number of IFHs belonging to each cluster: (a) 40, (b)	
	9, (c) 5, (d) 5	56

KEY TO SYMBOLS AND ABBREVIATIONS

CPT: Continuous Performance Task

CW: Choi-Williams

CWT: Continuous Wavelet Transform

EEG: Electroencephalogram

EP: Evoked Potential

FT: Fourier Transform

IF: Instantaneous Frequency

IFH: Instantaneous Frequency Histogram

PLV: Phase Locking Value

RID: Reduced Interference Distribution

SPS: Single Trial Phase Synchrony

STFT: Short-Time Fourier Transform

TFD: Time-Frequency Distribution

CHAPTER 1

INTRODUCTION

1.1 Problem Statement

Cognitive acts require the integration of numerous functional areas widely distributed over the brain and in constant interaction with each other. These interactions among separate areas of the brain are referred to as functional integration [1]. Recent research [2] suggests that the phase synchronization of signals transmitted along reciprocal connections between different areas of the brain allow for functional integration to occur. Numerous clinical trials have demonstrated that the phase synchronization of brain signals is related to functional integration [2]. In addition, results from Rodriguez et al. [3] show that phase synchrony is a better indicator of functional integration than amplitude dependent measures such as energy.

Furthermore, with the advance of neuroimaging technology, it is now possible to identify the oscillations of neuronal networks at high temporal and spatial resolutions, using multichannel recordings. Simultaneous recording of multiple oscillations between different cortical regions offers insight into how distributed neuronal oscillations interact with each other. These interactions, which can be used to study large-scale functional integration, are transient, time-varying, and frequency specific.

Therefore, there is a need for dynamic, high resolution phase synchrony measures to quantify the degree of functional integration that is occurring within the brain. Measures of phase synchrony must account for the nonstationary nature of brain signals. While some measures that use the Hilbert transform, short-time Fourier transform, or the continuous wavelet transform account for the nonstationarity of

the signals, they suffer from limited time and frequency resolution and scaling. In addition, current measures are limited because they can only quantify pairwise synchrony between neuronal oscillations, and cannot directly assess the large-scale interaction between groups of neuronal signals. For these reasons, there is a need for multivariate, high time-frequency resolution phase distributions based on Cohen's class for quantifying phase synchrony.

1.2 Contributions of Thesis

In this thesis, two new methods to measure phase synchrony are proposed. The first method uses a high resolution time-frequency phase distribution based on Cohen's class to measure time-varying phase estimation and phase synchrony between a pair of signals. The reduced interference Rihaczek distribution is proposed because of its abilities to measure complex energy and reduce cross-terms. The high resolution time-frequency distributions based on Cohen's class outperform other time-frequency distributions such as wavelets. Wavelets, on the other hand, use a non-uniform time-frequency resolution where the frequency resolution is high at low frequencies and low at high frequencies.

The second proposed method for measuring phase synchrony quantifies multivariate phase synchrony across groups of neuronal oscillations. Unlike previous multivariate methods [4], the proposed method uses distributions from Cohen's class with uniformly high time-frequency resolution. The proposed method is based on using the relationship between phase synchrony and frequency locking. Since phase and frequency are directly related to each other, two signals are synchronous whenever their instantaneous frequency is approximately the same. Using this relationship, an instantaneous frequency (IF) estimation method in the time-frequency domain is proposed to quantify the amount of synchronization between groups of signals. The IF estimates for different signals are combined using an instantaneous frequency

histogram (IFH) to indicate the amount of synchronization. The proposed method is then extended for multiple electrodes and multiple trial EEG recordings.

The proposed methods extend the state of the art in phase synchrony measures. Improved phase synchrony measures will help neuroscientists and psychologists understand functional integration within the brain, which is a vital aspect of proper brain function.

1.3 Organization of Thesis

This thesis is organized as follows. Chapter 2 reviews the background on EEG signals and time-frequency distributions. Chapter 3 presents and compares several techniques to measure the phase synchrony between a pair of signals. Chapter 4 proposes a new method to compute the phase synchrony over multiple electrodes and trials. Chapter 5 presents the results of applying the proposed methods to EEG signals collected during a study involving control and schizophrenic subjects. Finally, Chapter 6 discusses the contributions of this thesis along with some suggestions for future work.

CHAPTER 2

BACKGROUND

2.1 Electroencephalogram

The electroencephalogram (EEG) is a neuroimaging tool that measures the electrical potential over different areas of the brain. EEGs are non-invasive since the measurements are taken from a set of electrodes placed upon the scalp of the subject [5]. Each electrode measures the voltage signal generated by its respective area of the brain. The placement of the electrodes follows a predefined layout where each electrode is given a specific name [6].

EEG provides excellent temporal resolution compared to other neuroimaging methods at the expense of spatial localization. Some of the challenges of extracting useful information from EEG signals include low signal to noise ratio and volume conduction. EEG signals contain a large amount of "noise" because of the numerous activities that occur within the brain. Since the EEG measures voltages generated by the brain from an electrode on the scalp, the electric currents generated by the different areas of the brain can mix together during conduction through the skull and scalp resulting in the electrodes measuring a modified voltage signal from the original brain-generated signal. While most researchers choose to ignore volume conduction, others have developed techniques to reverse its effects on EEG signals. For example, the inverse EEG solution estimates the cortical activity from the EEG signals [2].

The EEG is commonly used in psychology and psychiatry to evaluate different psychopathologies. In these studies, a visual or audio stimulus is usually presented to the subject in order to measure the evoked potential (EP). In order to obtain reliable measurements of the evoked potential, the same stimulus is repeated multiple times

and the average EEG waveform, called the event related potential, is commonly analyzed.

EEG studies typically focus on specific time frames and frequency bands of interest. Some common time components of interest include P50, N100, P200, and P300. The 'P' indicates a positive deflection of the EEG during the time frame, and the 'N' indicates a negative deflection of the EEG. The number following the direction of the response corresponds to the latency in milliseconds of the deflection after the stimulus is applied to the subject. For example, the P300 time component includes the positive deflection of the EEG around 300 ms. In order to observe this deflection, the time frame from 200 to 600 ms after the stimulus should be analyzed. Furthermore, the frequency content of an EEG signal is roughly divided into 5 different frequency bands. Table 2.1 displays the approximate boundary frequencies of the different bands [6].

Table 2.1. The frequency bands of an EEG signal.

Band Name	Approx. Frequencies (Hz)
Delta (δ)	< 4
Theta (θ)	4-8
Alpha (α)	8-13
Beta (β)	13-30
Gamma (γ)	30-55

2.2 Functional Integration

The brain adheres to two fundamental principles of functional organization, functional integration and functional segregation, where the integration within and among specialized areas is mediated by effective connectivity [1]. Functional segregation is the functional specialization of a group of neurons. A single group of

neurons cannot perform cognitive processing independently. Instead, cognitive processing requires that the functionally and anatomically segregated areas of the brain must combine their functionality [7]. Recognizing a familiar face, for example, requires the functionality of both memory and vision. Functional integration refers to the interactions among the segregated neuronal areas and how these interactions depend upon cognition [1]. Functional integration is not static but is a dynamic and context dependent process.

The most likely mechanism for functional integration uses the strong reciprocal connections between different areas of the brain. It is believed that the phase synchronization of signals passed along these reciprocal connections allow for functional integration to occur in the brain [2]. The technical aspects of phase synchrony will be further discussed in Chapters 3 and 4. Numerous experiments on humans and animals using invasive and non-invasive techniques have demonstrated that phase synchronization plays a role in functional integration [8]. Rodriguez et al. [3] were one of the first to non-invasively demonstrate that phase synchrony occurs in the human brain during a cognitive task. They measured the phase synchrony of the EEG signals in the gamma band generated by a human subject during a facial perception task using 'Mooney' faces. The phase synchrony of the signals was found to be significantly greater when a face was perceived than when a face was not perceived. The type of phase synchronization recorded by EEGs is considered large-scale synchronization because of the long distances (> 1cm) between the electrodes. Besides the work performed by Rodriguez, Von Stein et al. [9] demonstrated the presence of long-range synchrony in the beta band of EEG signals from humans.

2.3 Time-Frequency Distributions

Most real life signals including EEG signals have time-varying frequency characteristics. Therefore, conventional signal processing methods based on time domain

modeling or frequency domain analysis are inadequate for the study of these signals. For example, the Fourier transform (FT) takes a signal from the time domain to the frequency domain. However, the transform cannot distinguish the frequency content of a signal at different time instances because it assumes the frequency characteristics of the signal are constant over the duration of the signal. In order to properly analyze the nonstationary EEG signals, a different signal analysis method must be utilized.

Time-frequency distributions (TFDs) represent a signal over both the time and frequency domains. This allows TFDs to handle signals with time-varying frequency characteristics. Figure 2.1 demonstrates the advantage of using a TFD over a FT for a complex exponential chirp signal defined as the following: $s(t) = \exp(j\pi(0.05 + 0.3t/400)t)$. The normalized frequency of the chirp signal increases linearly from 0.05 to 0.35. Given Figure 2.1(b), one is not able to determine that the instantaneous frequency of the signal is changing with time. All information about the time-varying frequency characteristics of the signal is lost by the FT. However, with the Wigner distribution in Figure 2.1(c), one is able to clearly determine that the signal's instantaneous frequency is linearly increasing in time. The Wigner distribution will be defined in Section 2.3.1.

The time frequency analysis methods of wavelets and TFDs have been used in the study of EEG signals in applications involving neurology and the study of psychopathologies. The work of Samar [10], Raz [11], and Basar [12] used wavelets to analyze event related potentials and resulted in a better understanding of the oscillatory characteristics of EEG. Several authors have used TFDs [13, 14, 15] or wavelets [16, 17] to detect and analyze epileptic seizures. Polikar has used wavelets to detect Alzheimer's disease [18, 19]. Other psychopathologies that have been analyzed using wavelets include schizophrenia [20] and obsessive compulsive disorder [21].

2.3.1 Cohen's Class of TFDs and the Wigner Distribution

Cohen's class of distributions are bilinear TFDs that are expressed as ¹[22]:

$$C(t,\omega) = \frac{1}{4\pi^2} \iiint \phi(\theta,\tau) s(u+\frac{\tau}{2}) s^*(u-\frac{\tau}{2}) e^{j(\theta u - \theta t - \tau \omega)} du d\theta d\tau \qquad (2.1)$$

where the function $\phi(\theta, \tau)$ is the kernel function and s is the signal. The kernel completely determines the properties of its corresponding TFD.

One of the most popular TFDs is the Wigner distribution with a kernel function of $\phi(\theta, \tau) = 1$. The Wigner distribution is a real-valued distribution that describes the energy of the signal over time and frequency, simultaneously.

The major differences between Cohen's class of TFDs compared to other time-frequency representations such as the wavelet transform are the nonlinearity of the distribution, energy preservation, and the uniform resolution over time and frequency. The wavelet transform provides a representation over time and scale where the frequency resolution is high at low frequencies and low at high frequencies. Although this property makes wavelet transform attractive in detecting high frequency transients in a given signal, it inherently imposes a non-uniform time-frequency tiling on the analyzed signal and thus results in biased energy representations. Cohen's class of bilinear TFDs on the other hand assumes constant resolution over the entire time-frequency plane. Figure 2.2 compares the time-frequency resolution of the wavelet transform and Cohen's class of TFDs.

2.3.2 Reduced Interference Distributions

One of the disadvantages of the Wigner distribution is the existence of cross-terms for multicomponent signals. Figure 2.3(a) displays the Wigner distribution for the sum of two Gabor logons. A Gabor logon is defined as a time and frequency shifted

 $^{^1}$ All integrals are from $-\infty$ to ∞ unless otherwise stated.

Gaussian window, $g(t) = (\frac{1}{\sigma^2 \pi})^{(1/4)} \exp(\frac{-(t-t_0)^2}{2\sigma^2}) \exp(j\omega_0 t)$. For this example, the sum of two Gabor logons signal, $s(t) = g_1(t) + g_2(t)$, is used with $t_{0,1} = 50$, $\omega_{0,1} = 0.7$, $t_{0,2} = 150$, and $\omega_{0,2} = 0.3$. As can be seen from the figure, apart from the individual energy distributions of the two logons, there are interference terms in the middle of the two auto-terms corresponding to the cross-terms. Attenuation of the cross-terms is possible through proper kernel selection and design. Distributions that reduce the presence of cross-terms are referred to as reduced interference distributions (RIDs).

To aid the kernel design process Equation 2.1 can be redefined into the following form:

$$C(t,\omega) = \frac{1}{4\pi^2} \iint \phi(\theta,\tau) A(\theta,\tau) e^{-j(\theta t + \tau \omega)} d\tau d\theta$$
 (2.2)

where $A(\theta, \tau)$ is the ambiguity function of the signal defined as:

$$A(\theta,\tau) = \int s(u + \frac{\tau}{2})s^*(u - \frac{\tau}{2})e^{j\theta u}du$$
 (2.3)

In the ambiguity domain the auto-terms of every component are located near the origin, while the cross-terms are located away from the origin. Therefore, in order to remove the cross-terms, a reduced interference kernel must be chosen with a passband around the origin. As a result, reduced interference kernels meet the following condition:

$$\phi(\theta, \tau) << 1 \quad \text{for } \theta \tau >> 0 \tag{2.4}$$

Figure 2.4 shows the ambiguity domain for the same sum of two Gabor logons. The desired auto-terms are located at the origin at the center of the figure, and the cross-terms are located off the axes.

The Choi-Williams kernel (CW) with $\phi(\theta,\tau) = \exp(-(\theta\tau)^2/\sigma)$ is an example kernel function that removes cross-terms by filtering in the ambiguity domain. The

resulting CW distribution can be written as the following:

$$C(t,\omega) = \iint \underbrace{\exp(-\frac{(\theta\tau)^2}{\sigma})}_{CW \text{ kernel}} A(\theta,\tau) e^{-j(\theta t + \tau\omega)} d\tau d\theta$$
 (2.5)

The value of σ can be adjusted to achieve a desired trade-off between resolution and the amount of cross-terms retained. Figure 2.3(b) displays the CW distribution with $\sigma = 4$ for the sum of two Gabor logons.

2.3.3 Rihaczek Distribution

Most of the members of Cohen's class are real valued energy distributions such as the Wigner and Choi-Williams distributions. These distributions are successful at describing the energy of the signal over both time and frequency. However, they do not carry any information about the phase of the signal. For this reason, they cannot be directly used for describing the phase information in an individual signal and estimating the phase synchrony between two signals.

In 1968, Rihaczek introduced the complex energy distribution and gave a plausibility argument based on physical grounds [23]. The Rihaczek distribution has a kernel function of $\phi(\theta, \tau) = \exp(j\theta\tau/2)$. Using the Rihaczek kernel reduces Equation 2.1 to the following:

$$C(t,\omega) = \frac{1}{\sqrt{2\pi}} s(t) S^*(\omega) e^{-j\omega t}$$
(2.6)

which is known as the Rihaczek distribution. This distribution measures the complex energy of a signal around time t and frequency ω . The complex energy density function provides a fuller appreciation of the properties of phase-modulated signals that is not available with other time-frequency distributions. The Rihaczek distribution is a bilinear, time and frequency shift invariant, complex-valued time-frequency distribution belonging to Cohen's class. The Rihaczek distribution provides both a time-varying energy spectrum as well as a phase spectrum, and thus is useful for

estimating the phase synchrony between any two signals.

2.3.4 Complex Continuous Wavelet Transforms

While complex continuous wavelet transforms (CWTs) are not part of Cohen's class of TFDs, they can be used as a benchmark during comparisons with the Rihaczek distribution. A popular complex CWT is the Morlet wavelet transform which is defined as the inner product of the signal, s(u), with the complex wavelet function [24]:

$$W(t,\omega) = \int s(u)\Psi^*(u)du \tag{2.7}$$

where $\Psi(u)$ is a Gaussian window shifted in time and frequency, and scaled proportional to the frequency:

$$\Psi(u) = \sqrt{\frac{\omega}{2\pi}} \exp(j\omega(u-t)) \exp(-\frac{(u-t)^2}{\sigma^2})$$
 (2.8)

with σ being inversely proportional to ω . The time-frequency scaling of the Morlet wavelet is nonuniform as previously demonstrated in Figure 2.2 because the variance, σ , changes with frequency. Also, the Morlet wavelet is similar to the short-time Fourier transform (STFT) where the window is defined as $h(u-t) = (\sqrt{\omega})\exp(j\omega t)\exp(-(u-t)^2/\sigma^2)$, which scales with respect to frequency, rather than as a Gaussian window, $h(u-t) = \sqrt{1/(2\pi\sigma^2)}\exp(-(u-t)^2/(2\sigma^2))$, which is constant with respect to frequency.

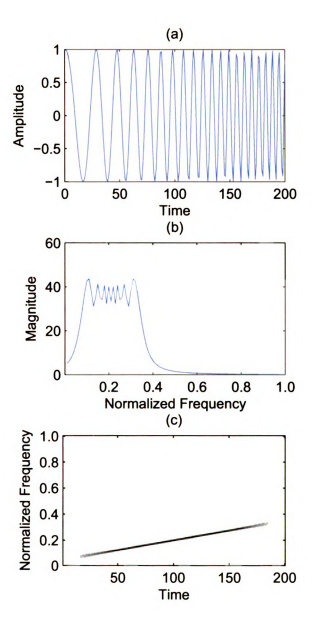


Figure 2.1. a) The real component of a complex exponential chirp signal that increases in normalized frequency from 0.05 to 0.35, b) the magnitude of the FT for the chirp signal, and c) the Wigner TFD of the same chirp signal.

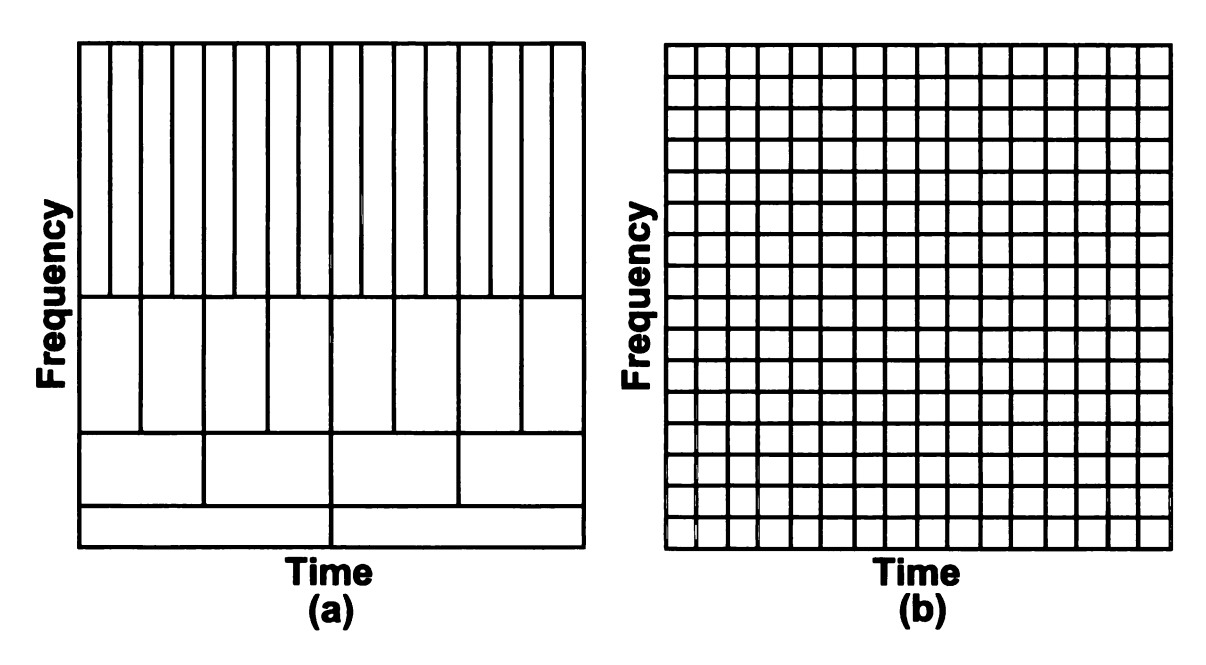


Figure 2.2. a) The non-uniform time-frequency resolution of the wavelet transform and b) the uniform time-frequency resolution of Cohen's class of TFDs.

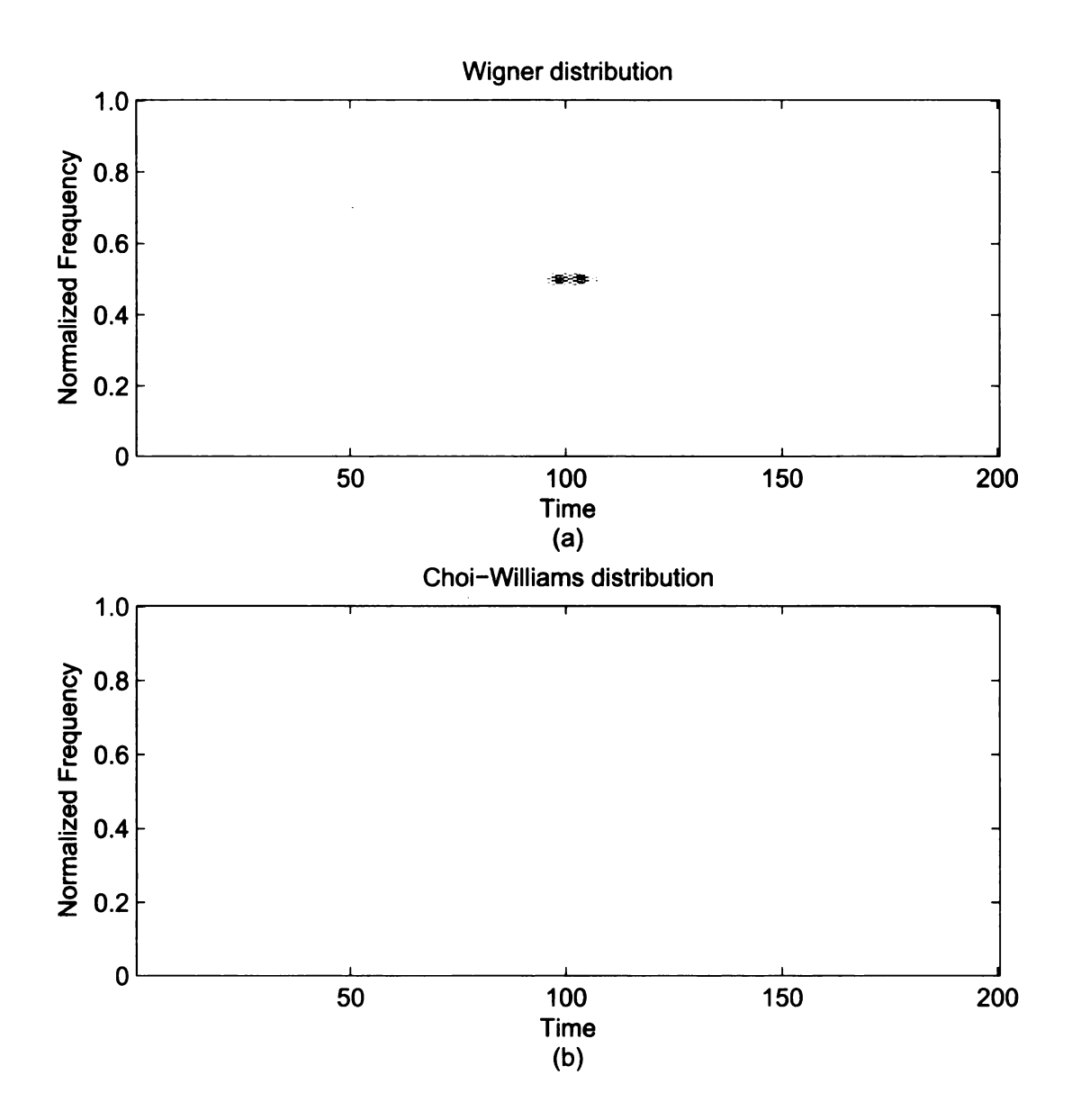


Figure 2.3. a) Wigner distribution and b) Choi-Williams distribution for the sum of two Gabor logons

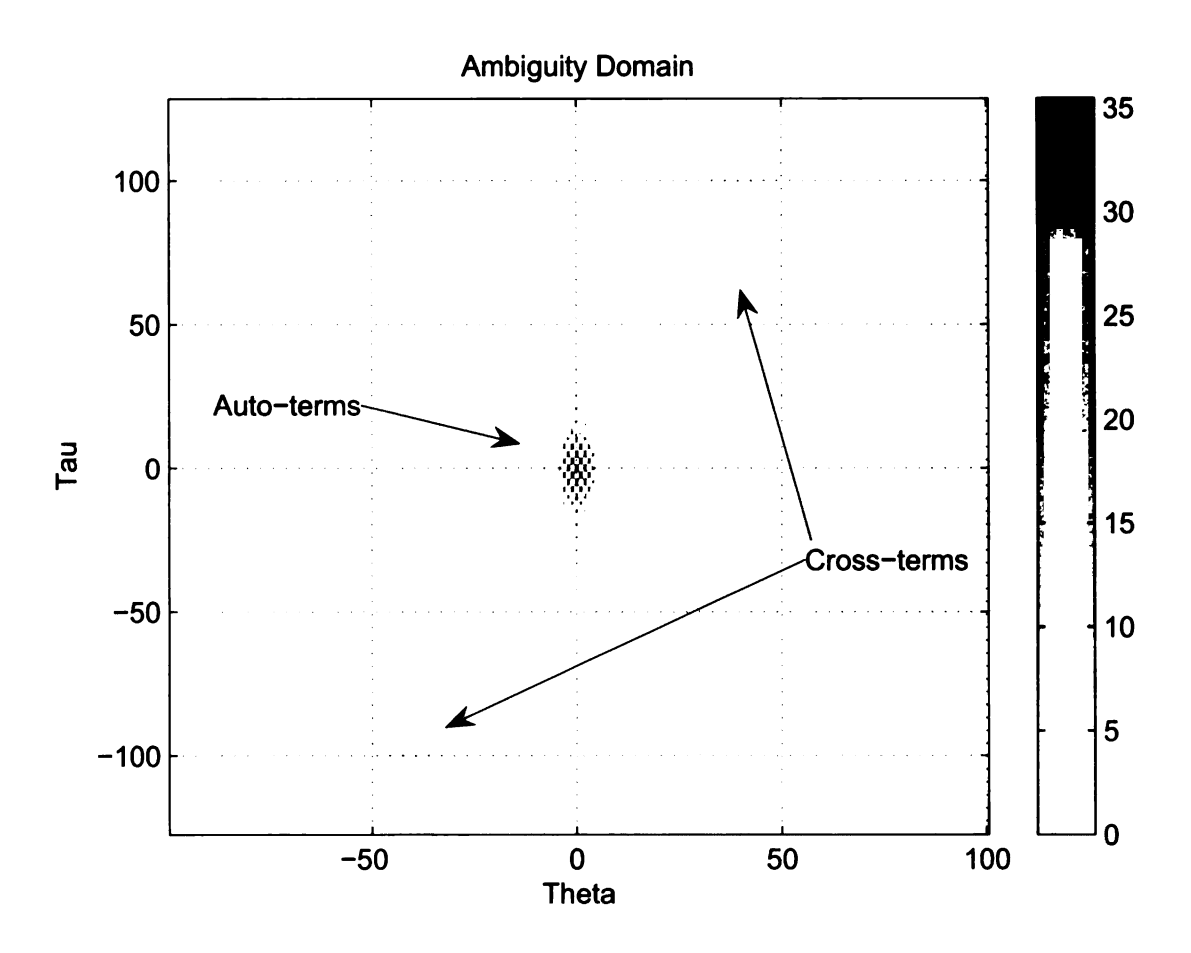


Figure 2.4. The ambiguity domain for the sum of two Gabor logons.

CHAPTER 3

BIVARIATE PHASE SYNCHRONY

As previously mentioned in Section 2.2, cognitive acts require the integration of numerous functional areas widely distributed over the brain and in constant interaction with each other. This integration is typically quantified by measuring the amount of phase synchrony between different regions of the brain. Bivariate phase synchrony measures the relation between the temporal structures of two signals regardless of the signal amplitude. Two signals are considered to be synchronous if their rhythms coincide.

3.1 Background on Phase Synchrony Measures

The most common measures used to quantify dependence between two signals is time domain cross-correlation [8] and spectral coherence [24]. The time-domain cross-correlation between two signals, x(t) and y(t), is defined as the following:

$$x(t) \star y(t) = \int x^*(u)y(t+u) du$$
 (3.1)

A high cross-correlation between two signals implies that the signals are similar. Cross-correlation is like covariance except that the signals are not shifted by their means. Also, the computation of cross-correlation is comparable to the computation of convolution except neither of the signals is reversed during cross-correlation [25]. The spectral coherence between the signals, x(t) and y(t), at a frequency of interest f is expressed as:

$$\varrho(f) = \frac{|S_{xy}(f)|}{[S_{xx}(f) \cdot S_{yy}(f)]^{1/2}}$$
(3.2)

where $S_{xy}(f)$ is the cross-spectral density between the signals x and y computed as the Fourier transform of the time-domain cross-correlation (Equation 3.1). However, these measures have limitations for two reasons. First, they assume stationarity of the underlying signals whereas most real life signals, including EEGs, are not. Second, coherence is a measure of spectral covariance and does not separate the effects of amplitude and phase from each other. The ideal phase synchrony measure should be able to separate the phase and amplitude effects from each other and take the nonstationary nature of brain activity into account [26]. The phase and amplitude terms of the input signals in Equations 3.1 and 3.2 can be separated into different components, but this change will not correct for the nonstationarity of the input signals.

In order to address these limitations, two different measures for quantifying phase synchrony have been proposed. In both methods, the amount of synchrony between two signals is usually quantified by first estimating the instantaneous phase of the individual signals around the frequency of interest. The first method employs the Hilbert transform to get the signal into an analytic form and estimates instantaneous phase directly from its analytic form [27]. In order to be able to estimate the instantaneous phase of a signal from its analytic form, one has to make sure that it is a narrow-band signal. For this reason, the Hilbert transform based phase synchrony measure first bandpass filters the signal around a frequency of interest and then uses the Hilbert transform to get the instantaneous phase. This is an indirect way of obtaining the frequency dependent phase estimates and is not exact. The second approach, on the other hand, computes a time-varying complex energy spectrum using either the CWT with a complex Morlet wavelet [24, 28] or the STFT [29] to get the phase of the signal.

For both phase synchrony measurements, the goal is to obtain an expression for the signal in terms of its instantaneous amplitude, a(t), and instantaneous phase, $\phi(t)$, at the frequency of interest as follows:

$$\tilde{s}(t,\omega) = a(t)\exp(j(\omega t + \phi(t))) \tag{3.3}$$

This formulation can be repeated for different frequencies and the relationships between the temporal organization of two signals, $s_1(t)$ and $s_2(t)$, can be observed by their instantaneous phase difference.

$$\Phi_{12} = |n\phi_1(t) - m\phi_2(t)| \tag{3.4}$$

where $\phi_1(t)$ and $\phi_2(t)$ are the phases of $s_1(t)$ and $s_2(t)$, respectively. In addition, n and m are integers that indicate the ratios of possible frequency locking. Most studies are only concerned about the case when n=m=1. In neuroscience, the focus is on the case when the phase difference is approximately constant over a limited time window. This is defined as a period of phase locking between two events. Phase locking is an indicator of the dynamic phase relationship between two oscillatory neuronal sources independently of their amplitude.

It has been observed that the two methods are similar in their results with the time-varying spectrum based methods giving sharper phase synchrony estimates over time and frequency, especially at the low frequency range [27]. Although the wavelet and STFT based phase synchrony estimates address the issue of non-stationarity, they suffer from a number of drawbacks. In the case of the wavelet transform, a representation over time and scale is obtained where the frequency resolution is high at low frequencies and low at high frequencies as was demonstrated by Figure 2.2. Despite this property making the wavelet transform attractive in detecting high frequency transients in a given signal, it inherently imposes a non-uniform time-frequency tiling on the analyzed signal and thus results in biased energy rep-

resentations and corresponding phase estimates. In the case of STFT, there is a tradeoff between time and frequency resolution due to the window. For these reasons, there is a need for high time-frequency resolution phase distributions that can better track the dynamic changes in phase synchrony.

3.2 Reduced Interference Rihaczek Distribution (RID-Rihaczek)

As mentioned in Section 2.3.3, the Rihaczek distribution is a complex-valued TFD from Cohen's class that provides phase information about the signal. Unfortunately, the Rihaczek distribution, like the Wigner distribution, suffers from the existence of interference terms for multicomponent signals. For any signal in the form, $s(t) = s_1(t) + s_2(t)$, the Rihaczek distribution is:

$$C(t,\omega) = \frac{1}{\sqrt{2\pi}} (s_1(t)S_1^*(\omega)e^{-j\omega t} + s_2(t)S_2^*(\omega)e^{-j\omega t} + s_1(t)S_2^*(\omega)e^{-j\omega t} + s_2(t)S_1^*(\omega)e^{-j\omega t})$$
(3.5)

where the last two terms in the above expression are the cross-terms. These cross-terms are located at the same time locations and occupy the same frequency bands as the original signals. A reduced interference Rihaczek distribution (RID-Rihaczek) must be defined to attenuate the cross-terms.

In Section 2.3.2, the CW kernel was used to filter the cross-terms in the ambiguity domain. After applying the CW kernel to the Rihaczek distribution, the resulting RID-Rihaczek can be written as [30]:

$$C(t,\omega) = \iint \underbrace{\exp(-\frac{(\theta\tau)^2}{\sigma})}_{\text{CW kernel}} \underbrace{\exp(j\theta\tau/2)}_{\text{Rihaczek kernel}} A(\theta,\tau)e^{-j(\theta t + \tau\omega)}d\tau d\theta \qquad (3.6)$$

where $A(\theta, \tau)$ is the ambiguity function of the signal as defined by Equation 2.3. This new distribution still satisfies the marginals and preserves the energy. Figure 3.1 illustrates the original and the reduced interference Rihaczek distributions using the same sum of two Gabor logons signal described in Section 2.3.2.

3.3 Time-Varying Phase Difference

The time-varying phase estimate of a signal based on the Rihaczek distribution can be defined as the following:

$$\Phi(t,\omega) = \arg\left[\frac{C(t,\omega)}{|C(t,\omega)|}\right],$$

$$= \arg\left[e^{j\phi(t)}e^{-j\theta(\omega)}e^{-j\omega t}\right],$$

$$= \phi(t) - \theta(\omega) - \omega t$$
(3.7)

where $\phi(t)$ and $\theta(\omega)$ refer to the phase in the time and the frequency domains, respectively.

Once the time-varying phase spectrum is defined, the phase difference between two signals, $s_1(t)$ and $s_2(t)$, with Rihaczek distributions of $C_1(t,\omega)$ and $C_2(t,\omega)$, respectively, can be computed as:

$$\Phi_{12}(t,\omega) = \arg \left[\frac{C_1(t,\omega)}{|C_1(t,\omega)|} \frac{C_2^*(t,\omega)}{|C_2(t,\omega)|} \right],$$

$$= \arg \left[e^{j((\phi_1(t) - \theta_1(\omega) - \omega t)} e^{-j(\phi_2(t) - \theta_2(\omega) - \omega t)} \right],$$

$$= \arg \left[e^{j((\phi_1(t) - \phi_2(t)) - (\theta_1(\omega) - \theta_2(\omega))} \right],$$

$$= (\phi_1(t) - \phi_2(t)) - (\theta_1(\omega) - \theta_2(\omega))$$
(3.8)

where $\phi_1(t)$ and $\phi_2(t)$ correspond to the phase of the time domain signals, whereas $\theta_1(\omega)$ and $\theta_2(\omega)$ correspond to the phase of the Fourier transform of the two signals, respectively.

It can be shown that for a real-valued signal, the phase between a signal $s_1(t)$

and its shifted version $s_1(t-t_0)$ is given by

$$\Phi_{12}(t,\omega) = \arg \left[\frac{s_1(t)S_1^*(\omega)e^{-j\omega t}}{|s_1(t)||S_1(\omega)|} \frac{s_1^*(t-t_0)S_1(\omega)e^{-j\omega t}0e^{j\omega t}}{|s_1(t-t_0)||S_1(\omega)|} \right],$$

$$= \arg \left[\frac{s_1(t)}{|s_1(t)|} \frac{s_1^*(t-t_0)e^{-j\omega t}0}{|s_1(t-t_0)|} \right],$$

$$= -\omega t_0$$
(3.9)

which is a linear function of frequency as expected.

Example: Time-Varying Phase Tracking: In this example, two complex exponential signals are considered with a time-varying phase difference, $x_1(t) = \exp(j\omega_1 t)$ and $x_2(t) = \exp(j\omega_1(t-at^2))$. Figure 3.2(a) illustrates the real component of the two signals. First, the Rihaczek distribution of the two complex exponentials is computed and then the phase difference between them is computed using Equation 3.8. Figure 3.2(b) compares the theoretical phase difference which is a second order polynomial and the estimated one at the frequency of interest, ω_1 . As can be seen from the figure, the proposed method is successful at estimating the time-varying phase difference with high accuracy. Images in this thesis are presented in color.

3.4 Measuring Bivariate Phase Synchrony

In most applications, the time-varying phase spectrum is not particularly useful for measuring the synchrony between signals. Similar to the definitions given in [24, 28, 31], phase synchrony measures based on the Rihaczek distribution time-varying phase estimate are defined. There are two major phase synchrony measures, single trial phase synchrony and phase locking value. Both of these measures are bivariate and therefore can only measure the phase synchrony between two signals.

3.4.1 Single Trial Phase Synchrony

Single trial phase synchrony (SPS) measures the phase locking between two electrodes averaged over time and is defined as:

$$SPS(t,\omega) = \left| \frac{1}{\delta} \int_{t-\delta/2}^{t+\delta/2} \exp(j\Phi_{12}(\tau,\omega)) d\tau \right|$$
 (3.10)

where δ is the length of the time window used for smoothing the phase difference estimates. In previous work based on the wavelet transform, δ is chosen as a function of frequency since the time-bandwidth product is not a constant for the wavelet transform. However, in the proposed approach, the phase synchrony is based on the time-frequency distribution which has a constant time-bandwidth product over the whole time-frequency plane. Therefore, δ will be a constant determined by the signal.

SPS will always be between 0 and 1, and can be used to detect neural synchrony between different parts of the brain. When the phase difference between the two signals is constant over time, SPS will be equal to 1.

3.4.2 Phase Locking Value

The phase locking value (PLV) is defined between two electrodes but is averaged over all trials. It measures the stability of phase differences across trials and is defined as:

$$PLV(t,\omega) = \frac{1}{N} \left| \sum_{k=1}^{N} \exp(j\Phi_{12}^{(k)}(t,\omega)) \right|$$
 (3.11)

where N is the number of trials and $\Phi_{12}^{(k)}(t,\omega)$ is the time-varying phase estimate between two electrodes during the kth trial. Like SPS, PLV ranges from 0 to 1.

3.4.3 Comparison Between the Wavelet and Rihaczek based Phase Synchrony Measures

In this example, we compare the performance of the PLV phase synchrony measure based on the complex Morlet wavelet transform and the Rihaczek distribution for signals with time-varying frequency content. Figure 3.3 compares the performance of wavelet based phase synchrony measure with Rihaczek based phase synchrony measure. With the Rihaczek based phase synchrony measure, the PLV is equal to 1 around the instantaneous frequency and smoothly tapers off as the frequency moves away from the instantaneous frequency. With the wavelet based phase synchrony measure, the PLV values do not taper off gradually but rather sharply and there is a larger bandwidth around the instantaneous frequency with a phase locking value of 1. It is also important to note that in the wavelet based phase locking value estimates, the bandwidth around the instantaneous frequency increases as the instantaneous frequency increases. This is due to the fact that at high frequencies the wavelet transform has high time resolution at the expense of low frequency resolution.

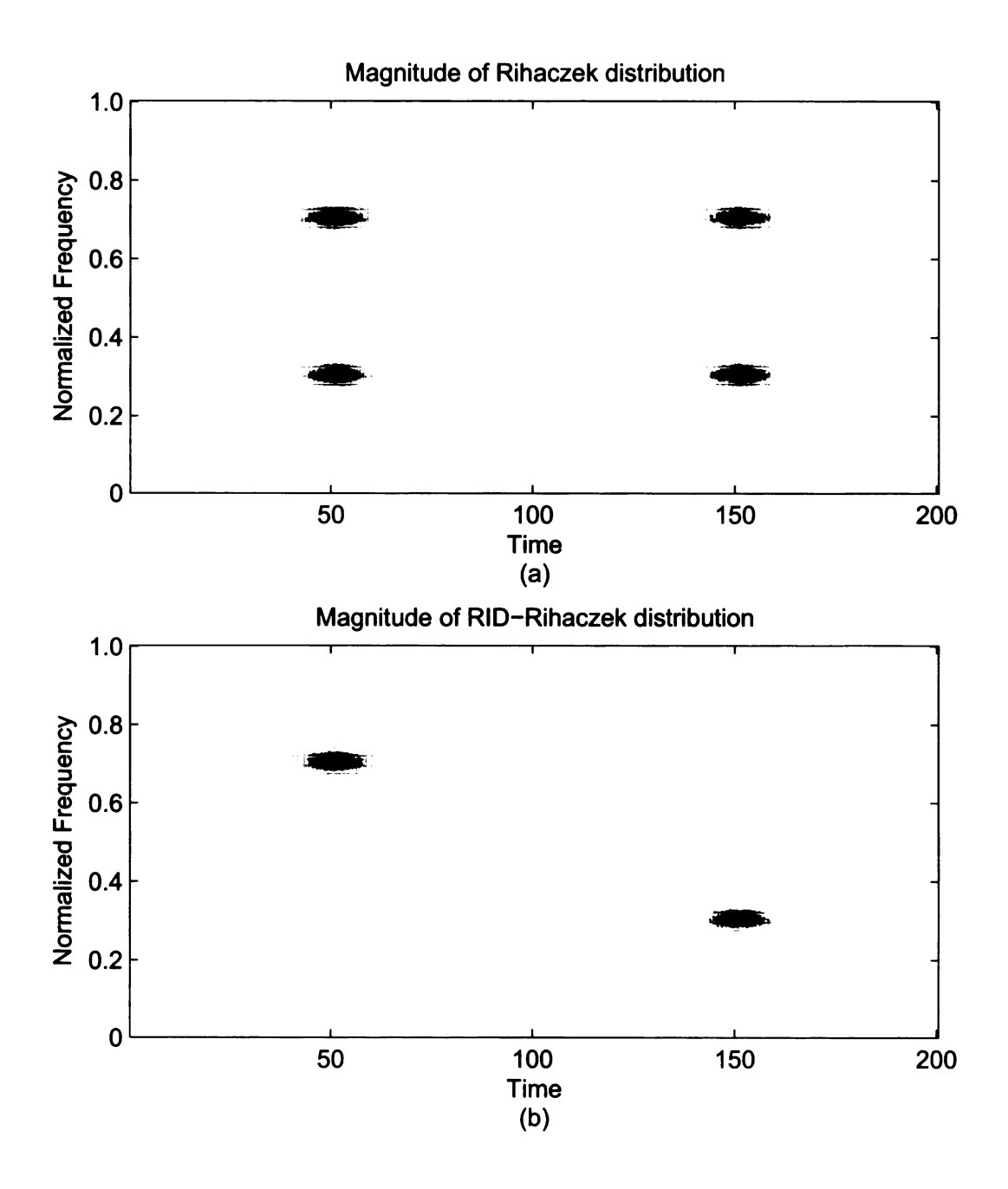


Figure 3.1. a) Magnitude of Rihaczek distribution and b) Magnitude of reduced interference Rihaczek distribution

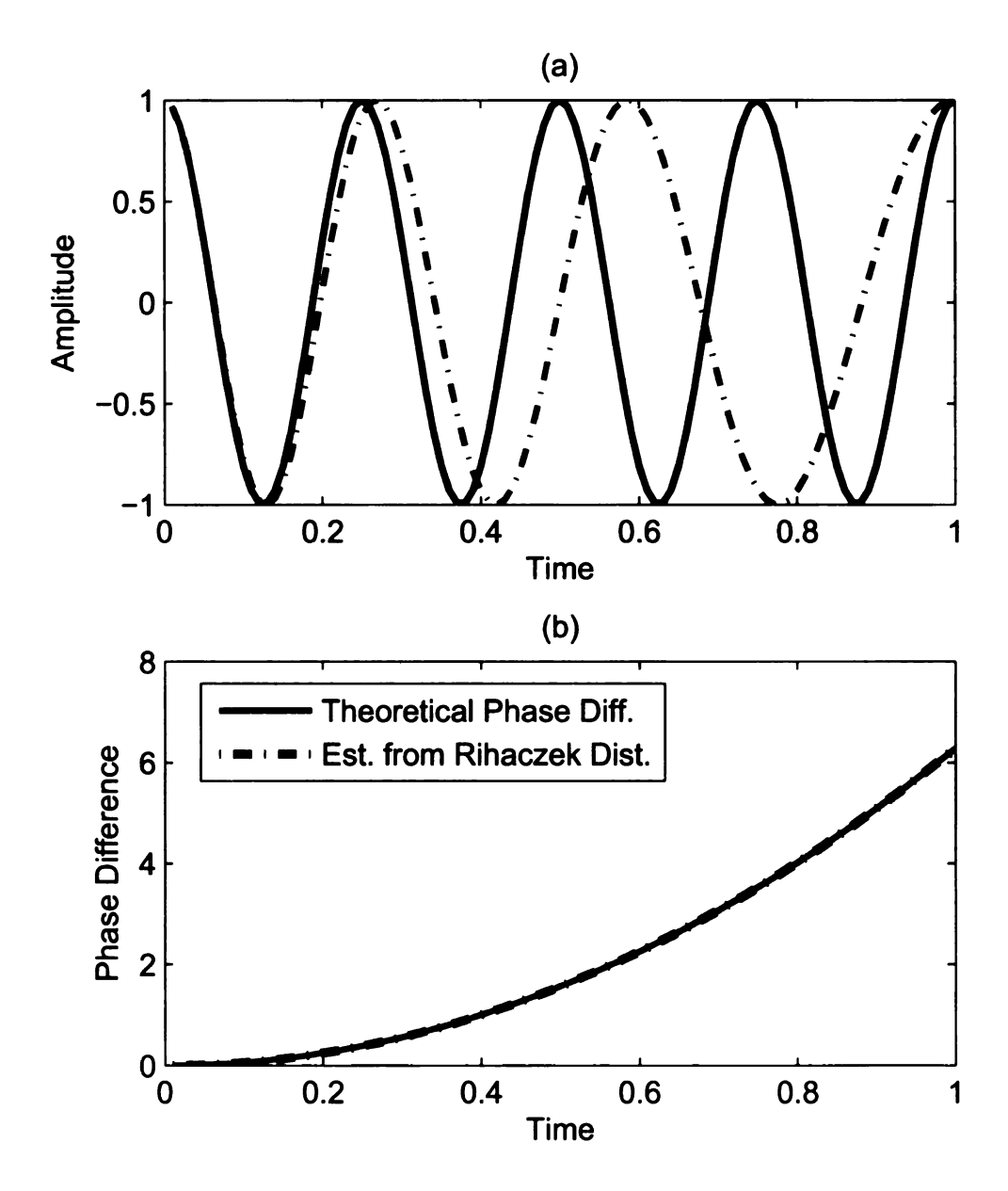


Figure 3.2. a) Real component of the two complex exponentials and b) Comparison of the theoretical and estimated time-varying phase difference of the two complex exponentials.

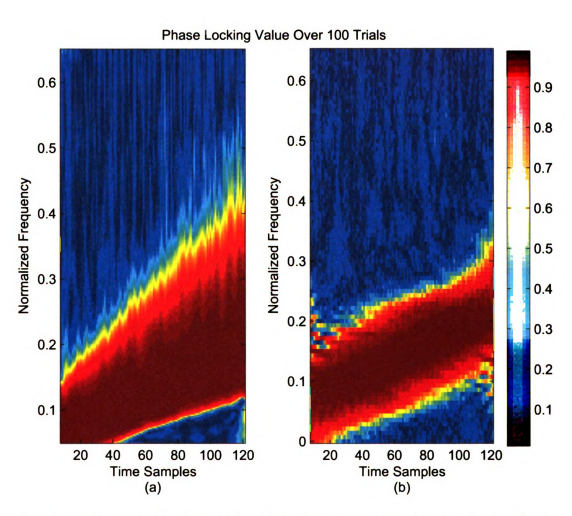


Figure 3.3. Average PLV for two chirps with a constant phase difference: a) wavelet distribution, b) Rihaczek distribution.

CHAPTER 4

MULTIVARIATE PHASE SYNCHRONY

Chapter 3 exclusively dealt with measures of phase synchrony between two signals at a time. Since most EEG signals involve multiple channels of data, the quantification of the relationships between different electrodes requires the computation of all possible pairwise synchronies. For example, 32 channel EEG will require the computation of 512 different bivariate phase synchrony combinations to determine the ensemble synchronization of the signals. In this chapter, a method will be presented to measure the phase synchrony between more than two signals. The proposed multivariate method is deterministic unlike the statistical methods described in Chapter 3.

The amount of research exploring multivariate phase synchrony has been relatively limited. Allefeld and Kurths developed a method to measure multivariate phase synchrony using statistical cluster analysis [32, 33]. Another technique developed by Rudrauf et al. estimates the instantaneous frequency of the signals with wavelets and finds common frequencies among the signals [4]. In this chapter, we will propose a multivariate phase synchrony measure based on the estimation of the instantaneous frequency of signals using high resolution time-frequency distributions.

4.1 Instantaneous Frequency

Two monocomponent analytic signals, $x_1(t) = a_1(t)e^{\phi_1(t)}$ and $x_2(t) = a_2(t)e^{\phi_2(t)}$, are phase synchronous if the phase difference between the two signals is constant. To allow for a small amount of noise in the phase of synchronous signals, the phase

difference can be approximately constant:

$$\Delta\phi_{1,2}(t) = m\phi_1(t) - n\phi_2(t) \approx \text{constant}$$
 (4.1)

where m and n are any two integers, and $\Delta \phi_{1,2}$ is the phase difference between the two signals. The derivative of Equation (4.1) can be shown as:

$$\frac{\mathrm{d}\Delta\phi_{1,2}(t)}{\mathrm{d}t} = m\frac{\mathrm{d}\phi_{1}(t)}{\mathrm{d}t} - n\frac{\mathrm{d}\phi_{2}(t)}{\mathrm{d}t} = m\omega_{1}(t) - n\omega_{2}(t) \approx 0 \tag{4.2}$$

where $\omega_i(t) = \frac{\mathrm{d}\phi_i}{\mathrm{d}t}(t) > 0$ and $w_i(t)$ is the instantaneous frequency (IF) of $x_i(t)$ in radians/second. Therefore, when n = m, two monocomponent signals are phase synchronous if they have approximately the same IF. This relation can be extended to three or more monocomponent signals. If a set of signals all have approximately the same IF, then all of the signals in the set are phase synchronous together [4].

The IF of a monocomponent signal can be computed by taking the time derivative of the phase of the analytic signal. Unfortunately, most real life signals, including brain signals, are not necessarily monocomponent. They tend to be multicomponent and are approximately equivalent to separable components in the following general form: $s(t) = \sum_k a_k(t)e^{j\phi_k(t)}$. While the same concept of phase synchrony applies to multicomponent signals, computing their IFs requires the use of more sophisticated methods [4].

4.2 Estimating IF of Multicomponent Signals

Ideally, the IF of a multicomponent signal will be the union of the IFs of the separate components. Numerous techniques exist to estimate the IF of a multicomponent signal. Previous methods include time-frequency moments, adaptive recursive least squares, and adaptive least mean square [34, 35]. Since most biological signals are non-stationary it is not possible to estimate their IF from the signal in the time

or frequency domain. For this reason, a time frequency (TF) peak algorithm for estimating IFs of multicomponent non-stationary signals is proposed.

For the purposes of IF estimation it is important to choose $\phi(\theta, \tau)$ such that it corresponds to a reduced-interference distribution in order to remove the cross-terms. The Choi-Williams distribution, previously mentioned in Section 2.3.2, is used to estimate the IF [22]. The proposed TF peak method can be summarized as follows:

- 1. Using the Choi-Williams kernel, compute the TFD of the signal, s(t), to get C(t,f).
- 2. Find the local peaks of C(t, f) using the following:

$$B(t,f) = \begin{cases} 1 & \text{if } \{\frac{\partial C(t,f)}{\partial f} = 0\} \land \{\frac{\partial^2 C(t,f)}{\partial f^2} < 0\} \\ 0 & \text{otherwise} \end{cases}$$
(4.3)

where B(t, f) is a binary-valued image with ones at the local peaks of C(t, f) and zeros everywhere else.

- 3. Assign all nonzero time-frequency points into connected components. A connected component D contains nonzero time-frequency points such that there is an 8-neighborhood path containing only points in D. Two time-frequency points are connected if $B(t_1,f_1)=1$, $B(t_2,f_2)=1$, $|t_2-t_1|\leq 1$, and $|f_2-f_1|\leq 1$.
- 4. Remove any connected component, D_i , from B(t, f) if $|D_i| < \epsilon$ where $|D_i|$ is the support of D_i . The removal of connected components with a small support reduces the effect of noise in s(t). The threshold, ϵ , is dependent on the application and the time support of the signal.

5. Compute the average energy of each component, D_j , as follows:

$$\xi_{j} = \frac{1}{|D_{j}|} \sum_{(t,f) \in D_{j}} C(t,f) \tag{4.4}$$

Remove any connected component, D_i , from B(t,f) if $\xi_i < \lambda$. The removal of low energy connected components reduces the effect of noise in s(t). The threshold, λ , is application dependent and should depend on the maximum average energy component.

The remaining connected components of B(t, f) form the IF estimate, $\hat{F}(t, f)$, of s(t). The resulting $\hat{F}(t, f)$ is a binary image with ones indicating the time and frequency location of the IF.

Consider the following example of estimating the IF for a multicomponent signal. The signal $x(t) = \sin(2\pi(3+3t)t) + \sin(24\pi t)$ contains two different components, a chirp and a sinusoid. The expected IF of the first component is $f_1(t) = 6t + 3$, and the expected IF of the second component is $f_2(t) = 12$. Figure 4.1 displays the expected and estimated IFs computed using the TF peak finding method.

4.3 Instantaneous Frequency Histograms

Given the fact that phase synchronous signals have similar IFs, the phase synchrony of multiple signals or multivariate phase synchrony can be represented using an instantaneous frequency histogram (IFH). If the collection of signals contains Q signals, computing the IF for each signal results in Q different IF estimates, $\hat{F}_i(t, f)$ for i = 1, 2, ..., Q. Summing the IFs from the collection of signals results in the IFH, IFH $(t, f) = \sum_{i=1}^{Q} \hat{F}_i(t, f)$. Since the IF estimate is a binary image, each value of the IFH is a discrete, finite value in the range from 0 to Q. For a single trial EEG consisting of multiple electrodes, the IFH represents the multivariate phase synchrony of the trial.

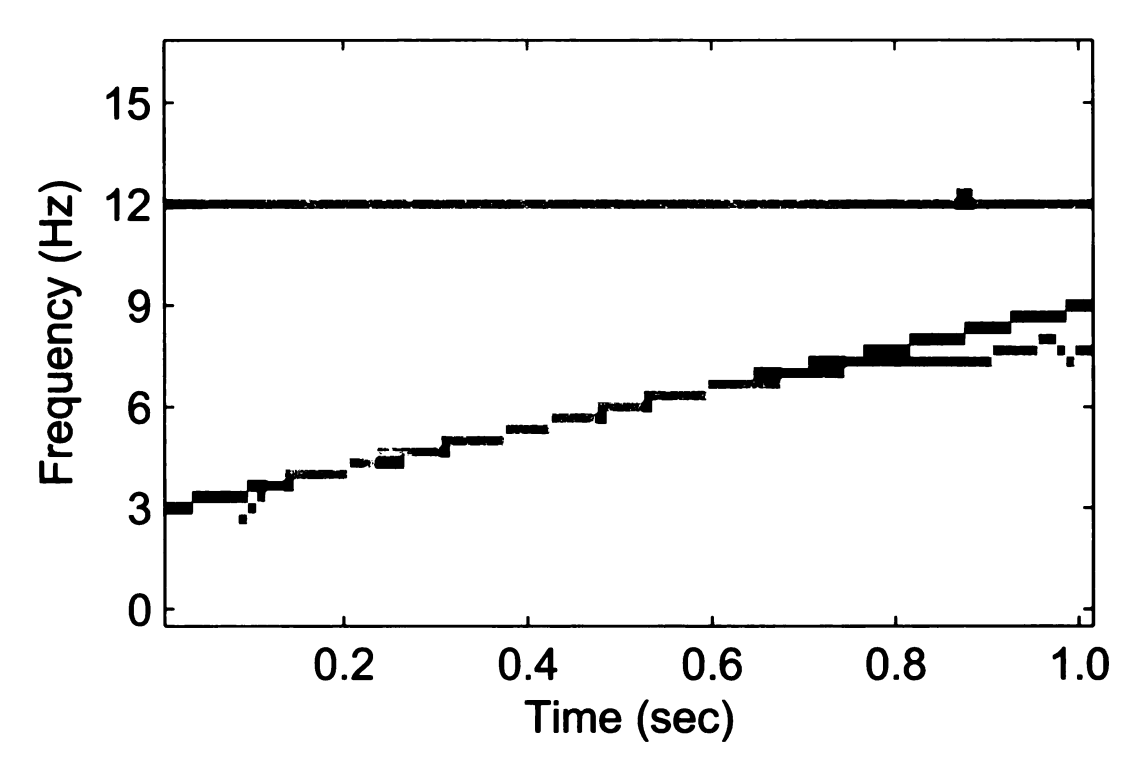


Figure 4.1. Example of estimating IF on a multicomponent signal. Black indicates the expected IF, and gray indicates the estimated IF.

4.4 Multiple Trial IFHs

Most EEG studies involve multiple trials of the same stimulus. Therefore, an EEG recording with N trials will result in N IFH surfaces across the electrodes. Each of the IFHs must be interpreted and analyzed to find general patterns of multivariate phase synchrony among the trials. Using data reduction techniques on the IFHs will determine representative patterns of multivariate phase synchrony across trials.

Typically, principal component analysis (PCA) is the primary tool for the dimension reduction of data sets. However, because of the discrete, finite values of the IFH, PCA is not the best option. For this reason, the K-means clustering approach is proposed for reducing the N IFH surfaces across trials into a few, distinct IFH components. The centroids can be restricted to the finite values of the IFH. For

K-means clustering, each time-frequency point of the IFHs is treated as a separate dimension in the clustering vector space, and each of the N IFHs is treated as a point in the clustering vector space. For indices i = 1, 2, ..., N and j = 1, 2, ..., K, K-means clustering can be summarized as follows:

- 1. Choose the initial centroids, $M_j = \text{median}(\{\text{IFH}_i : \text{IFH}_i \in R_j\})$ where R_j is a collection of randomly selected IFHs from the set of N IFHs.
- 2. Assign each IFH to a cluster by finding its nearest centroid $C_i= {\rm argmin}_j \, \|{\rm IFH}_i-M_j\|_2$, where C_i is the cluster index that ${\rm IFH}_i$ is assigned to.
- 3. Calculate the new centroids based upon the new cluster assignments using $M_j = \text{median}(\{\text{IFH}_i : C_i = j\}).$ The median is used rather than the mean to keep the centroids in the finite field.
- 4. If the centroids, M_j , have changed since the last iteration, go back to step 2. If the centroids, M_j , have not changed since the last iteration, stop.

The results of the K-means algorithm depend on the randomly chosen initial centroids. Multiple instances of the K-means clustering should be performed with different initial centroids, and the resulting relationships between the IFHs can be hierarchically clustered together to get a more stable clustering. Multiple K-means clusterings can be combined into a connection matrix using the following technique:

- 1. Define A to be a $N \times N$ connection matrix that is initially a zero matrix.
- 2. Perform the K-means algorithm on the N IFHs to get K different clusters.
- 3. For each $t=2,3,\ldots,N$ and $s=1,2,\ldots,t-1$, if IFH_s and IFH_t are in the same cluster such that $C_s=C_t$, then increment A(s,t). The matrix A will be upper triangular because s is always less than t.

4. Repeat steps 2 and 3 P-1 more times where P is the desired number of times that K-means clustering is performed. Each value of the connection matrix, A(s,t), is an integer ranging from 0 to P which indicates the number of times that IFH_s and IFH_t were in the same cluster.

Hierarchial clustering can now be performed on the connection matrix, A, by the following:

- 1. Assign each IFH to its own individual cluster by letting the cluster index $C_i = i$ for i = 1, 2, ..., N.
- 2. Find the location of the maximum value in A using $(s_max, t_max) = \arg\max_{s,t} A(s,t)$. If IFH_{s_max} and IFH_{t_max} are already in the same cluster such that $C_{s_max} = C_{t_max}$, then no action is necessary. However, if IFH_{s_max} and IFH_{t_max} are not in the same cluster such that $C_{s_max} \neq C_{t_max}$, then the clusters that contain IFH_{s_max} and IFH_{t_max} must be merged together. Merging can be performed by the following:

$$C_i = C_{s_max} \quad \text{if } C_i = C_{t_max} \tag{4.5}$$

for i = 1, 2, ..., N. The merge reduces the number of clusters by one.

- 3. Set $A(s_max, t_max) = 0$.
- 4. Return to step 2 if the number of different clusters is greater than K.
- 5. Compute the centroids by using $M_j = \text{median}(\{\text{IFH}_i : C_i = j\})$ for i = 1, 2, ..., N and j = 1, 2, ..., K.

Once the final clustering is complete, the significance of each centroid is determined by the number of IFHs in that cluster.

4.5 Quantifying IFHs

In order to quantify the phase synchrony from IFHs the correlation average is computed [4]:

$$pavg = \frac{\sum_{(t,f)\in W} (IFH^2(t,f) - IFH(t,f))}{n_c(n_c - 1)n_T n_F}$$

$$(4.6)$$

where n_c is the number of signals, W is the time-frequency window of interest, n_T is the number of time samples in W, and n_F is the number of frequency samples in W. The p_{avg} is an indicator of phase synchrony per TF point. An IFH with a higher p_{avg} indicates more signals are phase synchronous. In order for p_{avg} to be one, all time-frequency points in the window of interest need to be equal to n_c , which only occurs when every signal is phase synchronous at every time-frequency point in the window of interest. The window of interest, W, allows for the measure to be localized to a specific region of the TF plane.

4.6 IFH of Synthetic Signals

In this example, two sinusoidal signals are considered that are shown in Figure 4.2, $x_1(t) = \sin(2\pi f_1(t) + 2\pi/3)$ and $x_2(t) = \cos(2\pi f_2(t))$ where $f_1(t) = 3u(t) + 3u(t - 2) - 6u(t - 3)$ and $f_2(t) = 3u(t) - 3u(t - 1) + 6u(t - 2) - 6u(t - 3)$ such that u(t) is the unit step function. The sinusoids have the same IF of 3 Hz from 0 to 1 seconds and 6 Hz from 2 to 3 seconds. The resulting IFH in Figure 4.3 shows that the proposed method is effective at tracking the time-varying phase synchrony.

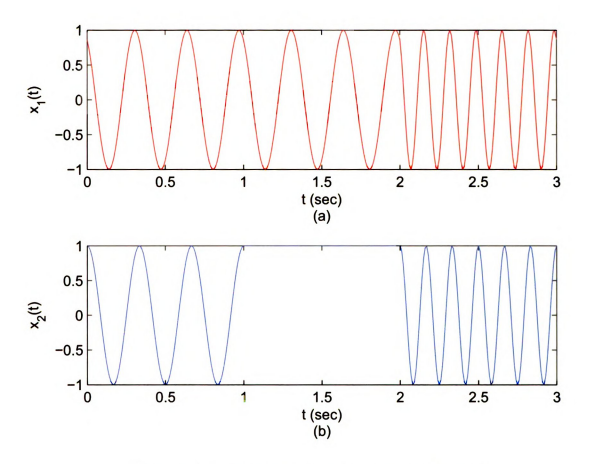


Figure 4.2. Synthetic signals (a) $x_1(t)$ and (b) $x_2(t)$.

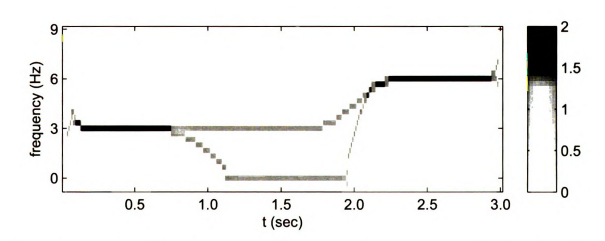


Figure 4.3. The IFH of a pair of synthetic signals with common IF from 0 to 1 seconds and from 2 to 3 seconds.

CHAPTER 5

RESULTS

In this chapter, the proposed bivariate and multivariate methods for measuring phase synchrony are applied to EEG signals, and the results are analyzed. Images in this thesis are presented in color.

5.1 Gamma Band Synchrony in Schizophrenic Subjects

One popular theory to the cause of schizophrenia is the reduced coordination of neural activities in the brain. This theory of schizophrenia is referred as the disconnection hypothesis by Friston [36]. Numerous postmortem studies have supported the disconnect hypothesis in schizophrenic subjects [37, 38]. Further research has shown that this theory of reduced coordination causes a lack of functional integration in the brain [39].

As previously mentioned in Section 2.2, functional integration in the brain is indicated by the amount of phase synchrony between neuronal populations. Furthermore, it has been found that oscillations in the γ band (30-55 Hz) are responsible for the coordination of neural activity [40, 41]. A schizophrenic subject with low levels of functional integration should have low levels of phase synchrony in the γ band. This hypothesis was shown to be true through experimentation by Spencer et al. [20] and Uhlhaas et al. [42] using a measure similar to PLV applied to the EEG data of control and schizophrenic subjects. The PLV measures used in these studies were based on the complex Morlet wavelet transform.

In this chapter, we test the hypothesis that schizophrenic patients have lower γ band synchrony for four schizophrenic and four non-psychiatric control subjects using the measures defined in Chapters 3 and 4. We have a total of 329 EEG trials for the four schizophrenia subjects and a total of 344 trials for the four control

subjects.

5.2 Bivariate Phase Synchrony in Schizophrenic Subjects

The γ band synchrony over 27 different electrodes is compared for the schizophrenic and control subjects during a cognitive task. The PLV is computed using Equation 3.11 over the P300 window (200-600 ms after the stimulus) and the γ band over all trials. Figure 5.1 and Figure 5.2 for the control and schizophrenic subjects show the PLV for all electrode pairs averaged over subjects, trials, and the time-frequency window, respectively. The electrode pairs with high PLV for both the control and schizophrenic subjects include C3-C3P, C4-C4P, P3-Pz, and P4-Pz. All of these electrode pairs are located in the central and parietal regions of the brain. The PLV of these electrode pairs are large likely because of the short physical distances between the electrodes.

To give a better insight into the results, the difference of the average PLV between the control and schizophrenic subjects is computed and shown in Figure 5.3. The difference between the two subject groups is highest for the electrode pairs C4-P8 and P4-P8. The control subjects have higher PLV for the electrode pairs in the central and parietal regions of the brain than the schizophrenic subjects. Spencer et. al also mentioned an increase of the phase synchrony in the parietal electrodes for the control subjects compared to the schizophrenic subjects in [20]. The increased PLV for the electrodes in the parietal region are likely caused by the stimulus being visual. However, for a few of the electrode pairs the schizophrenic subjects showed increased synchrony, specifically for the pairs: T8-FT8, F7-FT7, and T7-FT7, which are all located in the frontal and temporal regions of the brain.

The PLV over the time and frequency region with respect to electrode Fz averaged over subjects, trials, and the remaining 26 electrodes is shown for control and schizophrenic subjects in Figure 5.4 and Figure 5.5, respectively. The difference of

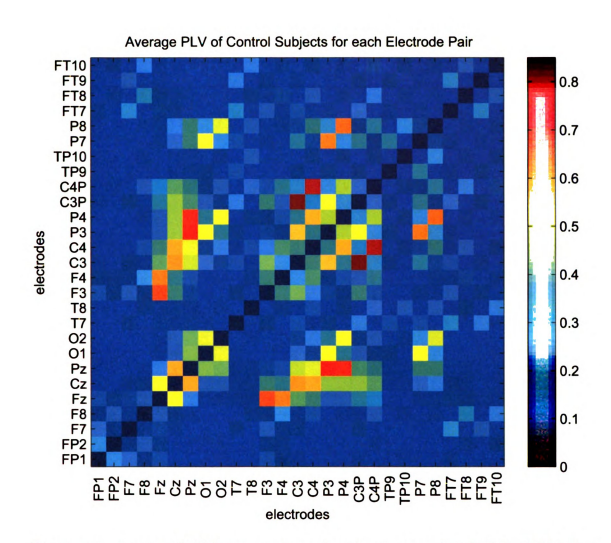


Figure 5.1. Average PLV between electrode pairs in the γ band of the P300 time window for the four control subjects. The diagonal of the figure, which is the PLV of an electrode with itself, is set to zero rather than one to improve scaling.

these two figures can be seen in Figure 5.6. The PLV of the schizophrenic subjects peaks at about 200 milliseconds after the stimulus in the frequency range 35 to 60 Hz. However, the PLV of the control subjects has higher peaks later in the P300 window. Also, the PLV for the control subjects appears highest in the 35 to 45 Hz frequency range. The higher PLV values for the control subjects become apparent when looking at the end of the P300 window in the difference figure (Figure 5.6) indicating increased γ band activity in the P300 window.

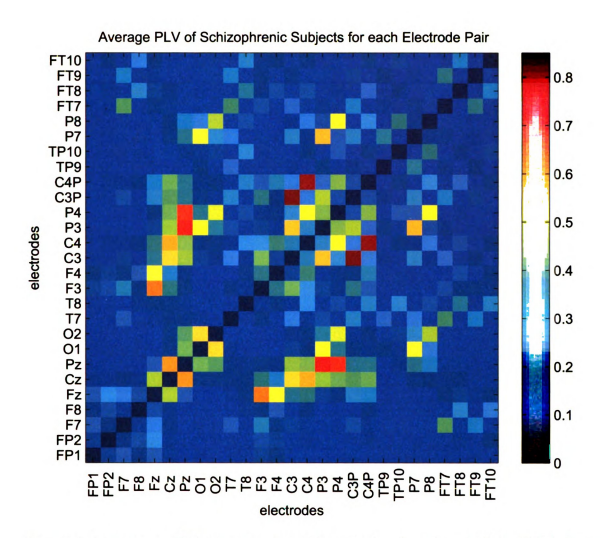


Figure 5.2. Average PLV between electrode pairs in the γ band of the P300 time window for the four schizophrenic subjects. The diagonal of the figure, which is the PLV of an electrode with itself, is set to zero rather than one to improve scaling.

A topo-map of the average PLV with respect to electrode Fz averaged over subjects, trials, and the time-frequency region (P300 time window, γ frequency band) is shown for control and schizophrenic subjects in Figures 5.7 and 5.8, respectively. The highest values of both topo-maps are found at electrodes F3, F4, and Cz. The difference of these two maps can be seen in Figure 5.9, which makes the results more apparent. As previously mentioned during the discussion of Figure 5.3, the control subjects have higher PLV in the central and parietal regions of the brain, but the

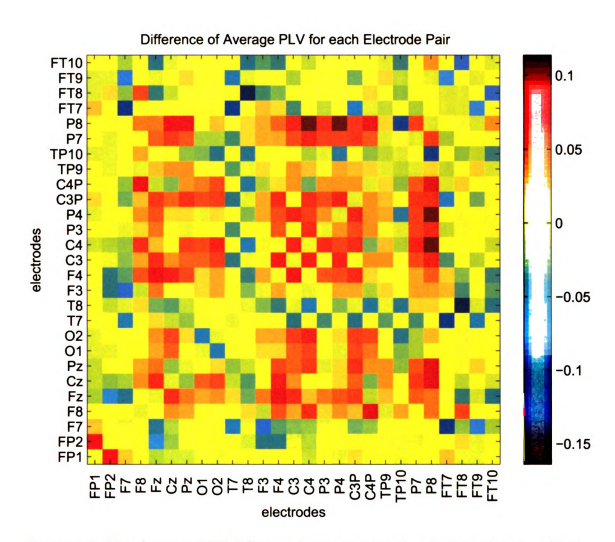


Figure 5.3. The Average PLV difference between control and schizophrenic subjects.

schizophrenic subjects show increased synchrony in the temporal and frontal regions of the brain. The difference topo-map matches this paradigm as well.

The statistical significance of the PLV measure can be shown by comparing it to the PLV measure using trial-shifted data [28]. The PLV for this surrogate data set is computed like the original PLV, but the phase difference is between two signals from a random permutation of the trials rather than two signals from the same trial.

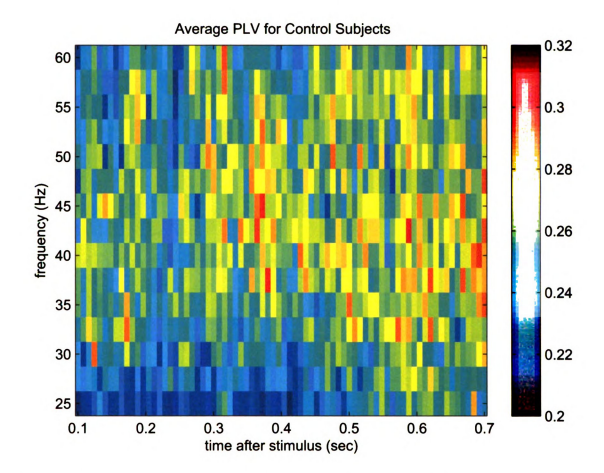


Figure 5.4. Average PLV with respect to electrode Fz for the four control subjects.

This computation can be seen in the following equation:

$$PLV_{surrogate}(t,\omega) = \frac{1}{H}\sum_{j=1}^{H}\frac{1}{N}\left|\sum_{k=1}^{N}\exp(j(\phi_{1}^{k}(t,\omega)-\phi_{2}^{perm(k)}(t,\omega)))\right| \quad (5.1)$$

where the constant H is the number of different random permutations. The $PLV_{surrogate}(t,\omega)$ is computed 200 times with a H of 40, which results in 200 different phase synchrony surfaces. The maximum of each one of these surfaces is taken to get 200 surrogate data thresholds. These 200 thresholds are compared to each time-frequency point's PLV value from the non-surrogate data set. The PLV measure is considered statistically significant if it is on average higher than 95% of

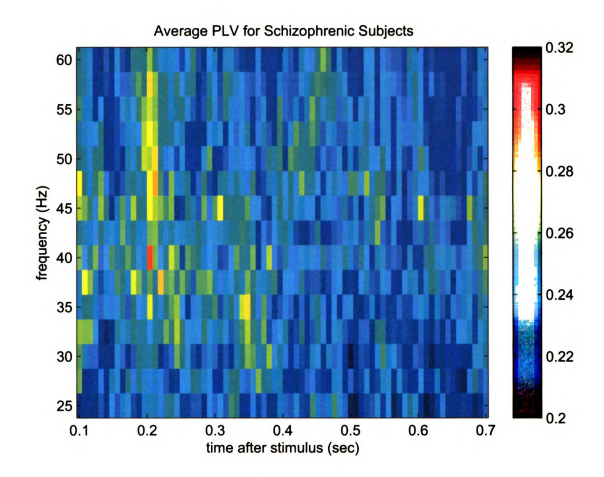


Figure 5.5. Average PLV with respect to electrode Fz for the four schizophrenic subjects.

the surrogate thresholds. Using this measure of statistical significance, it was found that the PLV measure is significant for both the control and schizophrenic data sets at all time-frequency points in the P300 time window and γ frequency band.

While the method described above shows that the PLV measure is significant, it does not show whether there is significant difference between the control and schizophrenic subjects based on the phase synchrony measure. The Student's t-test can be used to compare the significance of the PLV measure between control and schizophrenic subjects. The PLV was computed with respect to electrode Fz for each of the 26 remaining electrodes and each of the subjects averaged over the time range 500 to 700 ms after the stimulus and the 35-45 Hz frequency range. This

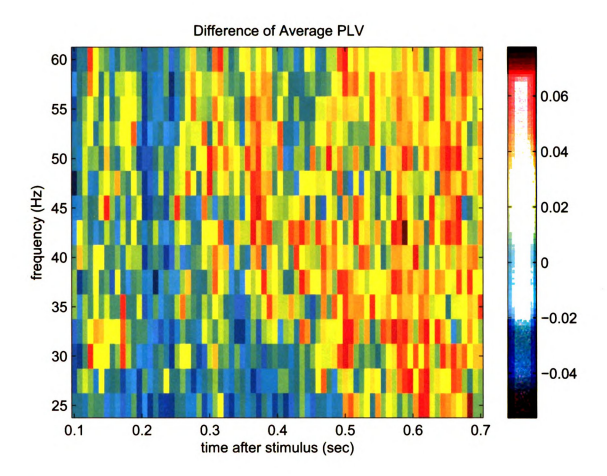


Figure 5.6. Difference of the average PLV with respect to electrode Fz between the control and schizophrenic subjects.

results in the control and schizophrenic subjects each having 26 different PLVs, one PLV for each electrode pairing. The t-statistic is computed using the samples, and the significance level is found by looking up the respective t-statistic in the t-table. Using this measure of statistical significance, it was found that the PLV for the control subjects is significantly higher than the PLV for the schizophrenic subjects at the $\alpha=0.1$ significance level. This corresponds to a late response time in the lower γ band.

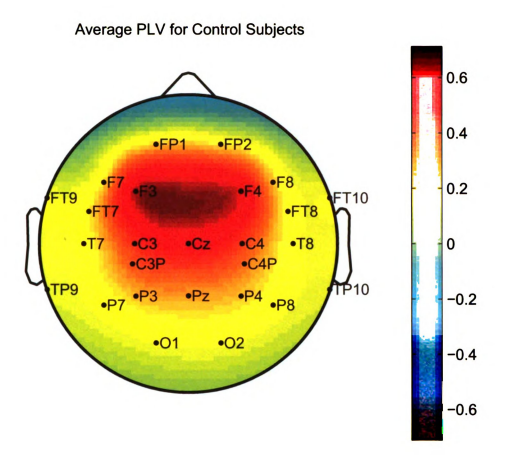


Figure 5.7. Topographic map of the average PLV with respect to Fz for four control subjects.

5.3 Multivariate Phase Synchrony in Schizophrenic Subjects

The PLV method used in the previous section is bivariate and, therefore, can measure the phase synchrony between only two electrodes. On the other hand, a multivariate method can measure the phase synchrony between more than two electrodes and will give a better indication of ensemble phase synchronization among the electrodes. The multivariate phase synchrony measure proposed in Chapter 4 is applied to 6 of the 27 electrodes. The six chosen electrodes (C3, C4, P3, P4, P7, and P8) are all from the central and parietal regions of the brain and were chosen based on

Average PLV for Schziophrenic Subjects

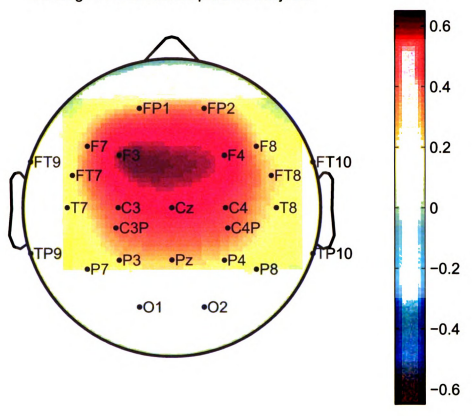


Figure 5.8. Topographic map of the average PLV with respect to Fz for four schizophrenic subjects.

their increased phase synchrony indicated by the bivariate results of Figure 5.3.

The IFHs for the multivariate method are computed with $\epsilon=10$ and $\lambda=0.05$ over the P300 window and the γ frequency band for the six chosen electrodes in each of the trials for all subjects. Multiple K-means clustering with K=40 and P=500 is then performed on the IFHs from the trials of each subject. This results in 8 different clusterings one for each subject, 4 control subjects and 4 schizophrenic subjects. Figures 5.9 through 5.13 display the four most significant cluster centroids for each control subject, and Figures 5.14 through 5.17 display the four most significant cluster centroids for each schizophrenic subject. The significance of a cluster

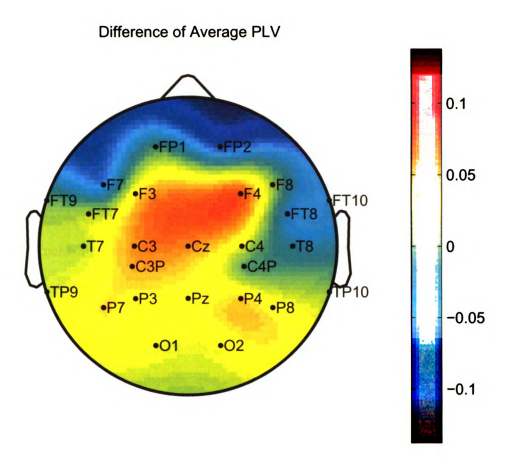


Figure 5.9. Topographic map of the difference of the average PLV with respect to Fz between control and schizophrenic subjects.

is determined by the number of IFHs in the cluster. The magnitude of the cluster centroids indicates the number of electrodes that were phase synchronous at that time-frequency point.

The top centroid of control subject 1, Figure 5.10(a), and control subject 2, Figure 5.11(a), contain most of their phase synchrony in the 40-50 Hz band with control subject 2 having four phase synchronous electrodes at 45 Hz. On the other hand, the top centroid of control subject 3, Figure 5.12(a), and control subject 4, Figure 5.13(a), contain most of their phase synchrony in the 50-55 Hz band. However, the second centroids of control subject 3, Figure 5.12(b), and control

subject 4, Figure 5.13(b), contain most of their phase synchrony in the 40-50 Hz band.

The top centroids of schizophrenic subject 2, Figure 5.15(a), and schizophrenic subject 4, Figure 5.17(a), contain relatively little phase synchrony in the γ frequency band. Schizophrenic subject 1 has some phase synchrony between two electrodes in the 50-55 Hz frequency band of the top centroid, Figure 5.14(a). Schizophrenic subject 3 is a notable exception among the schizophrenic subjects. This subject contains phase synchrony between three electrodes at the 45-55 Hz frequency band of its top centroid, Figure 5.16(a).

Tables 5.1 and 5.2 display the correlation averages (p_{avg}) , computed using Equation 5.2, in five different frequency bands for the four most significant centroids of the control and schizophrenic subjects, respectively. Table 5.3 shows the weighted average of the correlation averages, $\overline{p_{avg}}$, from each subject's four most significant centroids where the centroid's significance is used as the weight. The following equation shows how $\overline{p_{avg}}$ was calculated for each subject:

$$\overline{pavg} = \frac{\sum_{i=1}^{C} N^{(k)} p_{avg}^{(k)}}{\sum_{i=1}^{C} N^{(k)}}$$
(5.2)

where C is the number of clusters averaged over, $p_{avg}^{(k)}$ is the correlation average for the k-th cluster, and $N^{(k)}$ is the number of IFHs in the k-th cluster. An average of the $\overline{p_{avg}}$ is then taken over control and schizophrenic subjects, and the difference is taken between the control and schizophrenic subjects which can be seen at the bottom of Table 5.3.

From the difference row in Table 5.3 it can be seen that the control subjects have a higher correlation average than the schizophrenic subjects in the 40-50 Hz

frequency band. The higher correlation averages indicate that the control subjects show increased phase synchrony over the schizophrenic subjects in the six chosen electrodes in the P300 time window of the 40-50 Hz frequency band. However, the schizophrenic subjects do have a higher correlation average for the 50-55 Hz frequency band.

This result is similar to the results from the bivariate measure as seen in Figure 5.6. With the bivariate measure, the control subjects exhibited increased synchrony over the schizophrenic subjects in the 35-45 Hz frequency band rather than in the 40-50 Hz frequency band for the multivariate measure. However, the measures did not use the same electrode pairings. The bivariate measure in Figure 5.6 paired electrode Fz with the 26 other electrodes while the multivariate measure used the electrodes: C3, C4, P3, P4, P7, and P8. Despite this difference, the results are relatively similar.

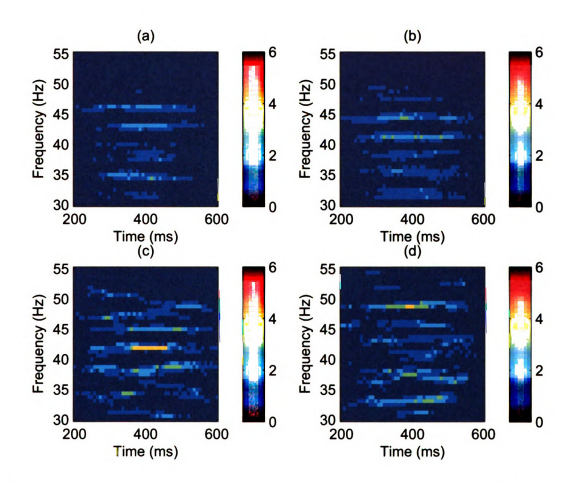


Figure 5.10. The four most significant cluster centroids of control subject 1. The number of IFHs belonging to each cluster: (a) 15, (b) 14, (c) 3, (d) 3.

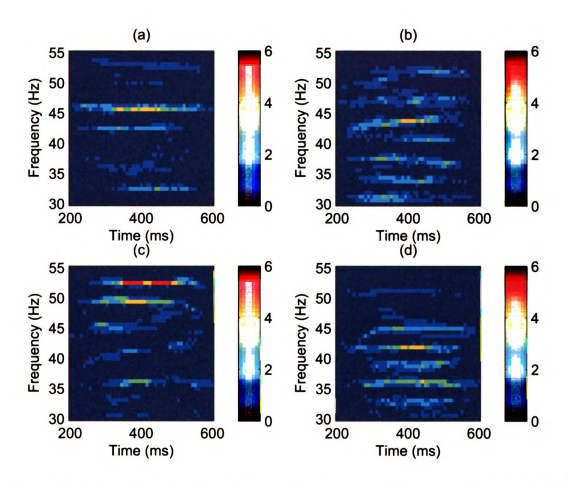


Figure 5.11. The four most significant cluster centroids of control subject 2. The number of IFHs belonging to each cluster: (a) 12, (b) 6, (c) 5, (d) 4.

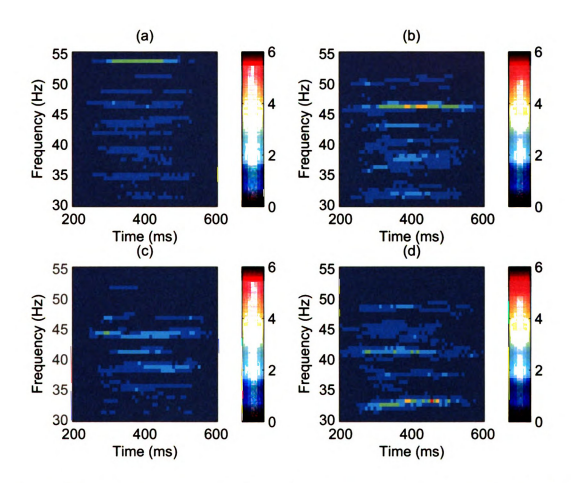


Figure 5.12. The four most significant cluster centroids of control subject 3. The number of IFHs belonging to each cluster: (a) 21, (b) 6, (c) 5, (d) 4.

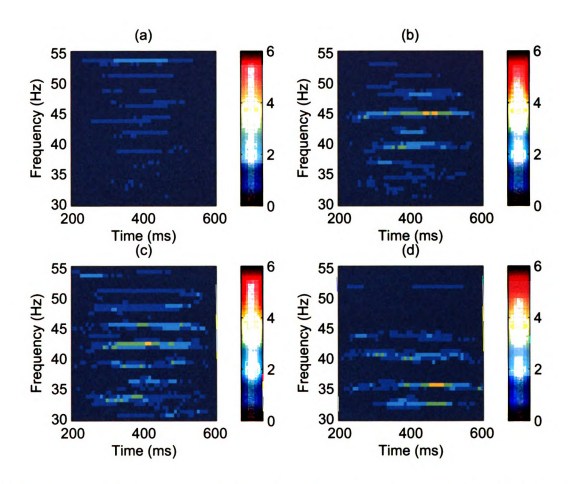


Figure 5.13. The four most significant cluster centroids of control subject 4. The number of IFHs belonging to each cluster: (a) 60, (b) 7, (c) 3, (d) 3.

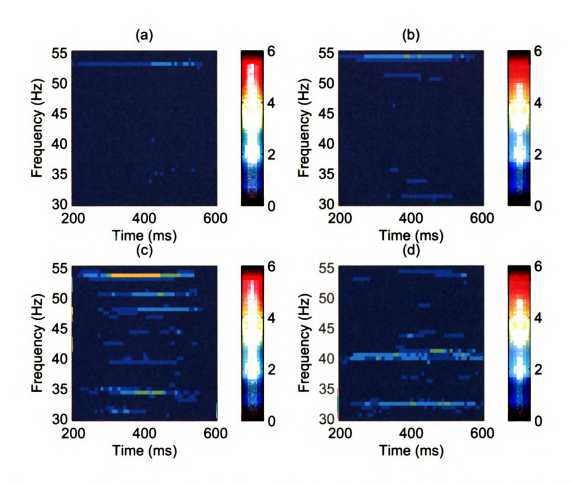


Figure 5.14. The four most significant cluster centroids of schizophrenic subject 1. The number of IFHs belonging to each cluster: (a) 27, (b) 21, (c) 5, (d) 3.

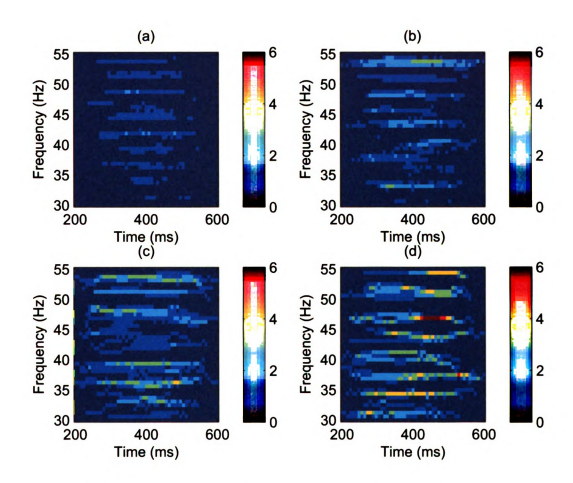


Figure 5.15. The four most significant cluster centroids of schizophrenic subject 2. The number of IFHs belonging to each cluster: (a) 32, (b) 8, (c) 2, (d) 1.

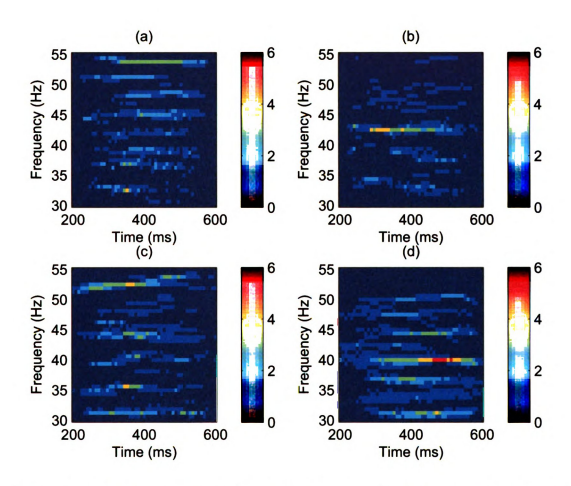


Figure 5.16. The four most significant cluster centroids of schizophrenic subject 3. The number of IFHs belonging to each cluster: (a) 5, (b) 3, (c) 3, (d) 2.

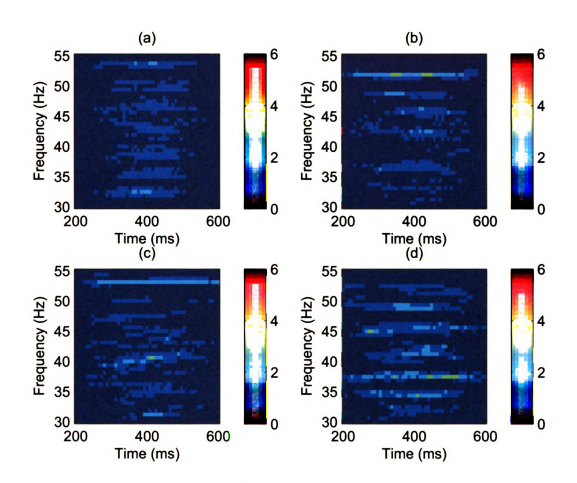


Figure 5.17. The four most significant cluster centroids of schizophrenic subject 4. The number of IFHs belonging to each cluster: (a) 40, (b) 9, (c) 5, (d) 5.

Table 5.1. The correlation averages in five different frequency bands for the four most significant centroids of each control subject.

Subject	Significance	p_{avg} by Frequency Band				
		30-35 Hz	35-40 Hz	40-45 Hz	45-50 Hz	50-55 Hz
Control 1	15/35	0.0031	0.0002	0.0028	0.0028	0.0000
	14/35	0.0003	0.0010	0.0106	0.0000	0.0000
	3/35	0.0034	0.0103	0.0201	0.0036	0.0007
	3/35	0.0095	0.0093	0.0021	0.0147	0.0002
Control 2	12/27	0.0036	0.0000	0.0039	0.0212	0.0000
	6/27	0.0096	0.0072	0.0175	0.0034	0.0028
	5/27	0.0000	0.0052	0.0021	0.0199	0.0330
	4/27	0.0033	0.0225	0.0201	0.0000	0.0000
Control 3	21/36	0.0000	0.0000	0.0000	0.0003	0.0100
	6/36	0.0020	0.0039	0.0025	0.0198	0.0000
	5/36	0.0002	0.0036	0.0095	0.0007	0.0000
	4/36	0.0150	0.0008	0.0070	0.0013	0.0000
Control 4	60/73	0.0000	0.0000	0.0000	0.0000	0.0031
	7/73	0.0000	0.0062	0.0162	0.0015	0.0000
	3/73	0.0062	0.0060	0.0176	0.0078	0.0015
	3/73	0.0077	0.0134	0.0049	0.0000	0.0000

Table 5.2. The correlation averages in five different frequency bands for the four most significant centroids of each schizophrenic subject.

Subject	Signif.	p_{avq} by Frequency Band				
		30-35 Hz	35-40 Hz	40-45 Hz	45-50 Hz	50-55 Hz
Schizophrenic 1	27/56	0.0000	0.0000	0.0000	0.0000	0.0018
	21/56	0.0000	0.0000	0.0000	0.0000	0.0062
	5/56	0.0069	0.0000	0.0002	0.0031	0.0265
	3/56	0.0074	0.0047	0.0095	0.0000	0.0003
Schizophrenic 2	32/43	0.0000	0.0000	0.0007	0.0005	0.0000
	8/43	0.0041	0.0015	0.0051	0.0039	0.0147
	2/43	0.0059	0.0263	0.0008	0.0131	0.0211
	1/43	0.0312	0.0284	0.0242	0.0337	0.0335
Schizophrenic 3	5/13	0.0029	0.0051	0.0038	0.0036	0.0157
	3/13	0.0016	0.0015	0.0160	0.0000	0.0000
	3/13	0.0078	0.0067	0.0078	0.0010	0.0175
	2/13	0.0105	0.0391	0.0075	0.0034	0.0013
Schizophrenic 4	40/59	0.0010	0.0000	0.0000	0.0000	0.0007
	9/59	0.0000	0.0002	0.0008	0.0018	0.0088
	5/59	0.0011	0.0013	0.0020	0.0000	0.0069
	5/59	0.0038	0.0095	0.0051	0.0052	0.0000

Table 5.3. The weighted average of the correlation averages for the four most significant centroids of each control and schizophrenic subject in five different frequency bands. The final row contains the difference between the average control subject's correlation average and the average schizophrenic subject's correlation average.

Subject	Weighted Avg p_{avg} by Frequency Band					
	30-35 Hz	35-40 Hz	40-45 Hz	45-50 Hz	50-55 Hz	
Control 1	0.0026	0.0022	0.0073	0.0028	0.0001	
Control 2	0.0042	0.0059	0.0090	0.0139	0.0067	
Control 3	0.0020	0.0012	0.0025	0.0037	0.0058	
Control 4	0.0006	0.0014	0.0025	0.0005	0.0026	
Schizophrenic 1	0.0010	0.0003	0.0005	0.0003	0.0056	
Schizophrenic 2	0.0018	0.0022	0.0021	0.0025	0.0045	
Schizophrenic 3	0.0049	0.0099	0.0081	0.0021	0.0103	
Schizophrenic 4	0.0011	0.0009	0.0007	0.0007	0.0024	
Control Avg.	0.0024	0.0027	0.0053	0.0052	0.0038	
Schizophrenic Avg.	0.0022	0.0033	0.0029	0.0014	0.0057	
Difference	0.0002	-0.0006	0.0024	0.0038	-0.0019	

CHAPTER 6

CONCLUSIONS AND FUTURE WORK

In this thesis, two different measures of phase synchrony, bivariate and multivariate measures, were introduced. The bivariate phase synchrony measure computes the phase locking value (PLV) using the reduced interference Rihaczek distribution between pairs of signals and gives a measure of the variability of phase differences across trials. The multivariate phase synchrony measure, on the other hand, is a deterministic measure of phase synchrony that is directly related to the instantaneous frequency. Multiple K-means clusterings are performed on the instantaneous frequency histograms in the time-frequency plane to estimate the phase synchrony across multiple electrodes.

6.1 Contributions

One of the major contributions of this thesis is the introduction of the reduced-interference Rihaczek distribution. Time-frequency distributions like the Wigner and Rihaczek distributions suffer from cross-terms when applied to multi-component signals. The reduced interference Rihaczek distribution removes the cross-terms by applying a Choi-Williams kernel in the ambiguity domain. In addition, the reduced interference Rihaczek distribution, like the Rihaczek distribution, is complex and retains the phase information unlike classical time-frequency methods such as the Morlet wavelet and Wigner distribution.

While previous bivariate measures computed the PLV using a different time-frequency distribution such as the Morlet wavelet, this thesis proposed using the reduced interference Rihaczek distribution to compute the PLV. The Morlet wavelet suffers from biased phase estimates because of its nonuniform frequency resolution. The reduced interference Rihaczek distribution, like all time-frequency distributions

in Cohen's class, has a uniform resolution and as a result has an unbiased phase estimate. The introduction of Cohen's class of time-frequency distributions to the computation of PLV is a major contribution of this thesis.

Another contribution is the proposed multivariate phase synchrony measure, which can be applied to multiple trials, unlike previous multivariate measures. Previous multivariate measures could only be applied to a single trial, and as a result every instantaneous frequency histogram (IFH) would have to be analyzed independently to get an overview of the phase synchrony across the trials. By applying K-means clustering to the IFHs, the major frequency locking patterns can be extracted and analyzed to give a general overview of the phase synchrony across the trials and electrodes.

6.2 Future Work

6.2.1 Multivariate Method Improvements

One disadvantage of the proposed multivariate method is the need for parameter calibration. The IF estimation requires two different parameters, the time support threshold (ϵ) and the average energy threshold (λ). These parameters determine which components are filtered out of the IF estimate. The time support threshold depends on the length of the signal, and the average energy threshold depends on the energy of the signal. Multiple K-means requires two additional parameters, the number of clusters (K) and number of times K-means clustering is performed (P). A larger P value gives a more accurate clustering. Both of these parameters depend on the number of trials and time-frequency points. An automated technique to optimize these parameters would significantly improve the efficiency of this method.

Furthermore, another disadvantage of the proposed multivariate method is the inability to determine which electrodes are phase synchronous. Only the number of electrodes that are phase synchronous are known from the IFH. This issue could

be solved by multiplying each electrode's IF estimate by a unique number that is a power of two. The resulting IFH can then be decoded to determine the original IF estimates from each electrode.

In addition, the multivariate method cannot be easily extended to multiple subjects. The cluster centroids cannot be averaged together because of their discrete finite values, and using K-means clustering on the IFHs from multiple subjects proved to be ineffective.

6.2.2 Volume Conduction

Volume conduction, which was first defined in Section 2.1, is the mixing of brain signals traveling from the brain to the electrodes on the scalp. A reduction of volume conduction would assure that only true phase synchrony is measured. The effects of volume conduction can be seen in the topo-maps of Figures 5.7 and 5.8. The electrodes around the reference electrode (Fz) have higher PLVs than the electrodes further away from the electrode.

Lachaux suggests two different techniques to reduce volume conduction, scalp current density and inverse deblurring [31]. The scalp current density is computed by multiplying the Laplacian of the EEG by the negative of the scalp conductivity [43]. Measures of phase synchrony can then be applied directly to the scalp current density. Inverse deblurring estimates the potentials of the cortical sources in a finite element model by optimizing the difference between the measured EEG data and the estimated potentials of cortical sources conducted through the skull and scalp [44]. Measures of phase synchrony can then be applied to the estimated potentials of the cortical sources. Another popular technique to reduce volume conduction is baseline correction, which subtracts the phase synchrony measure during the pre-stimulus from the phase synchrony measure during the P300 time window. The measure from the pre-stimulus should be mostly volume conduction, and by subtracting it from the measure during the P300 time window, the phase synchrony caused by volume

conduction will be removed.

6.2.3 Directional Measures

Neither of the measures presented in this thesis are directional. From directionality, the causality or the direction of the coupling could be determined. Pereda et al. [45] discuss several directionality measures such as transfer entropy, partial directed coherence, and Granger causality. However, none of these are measures of phase synchrony because they take the amplitude of the signals into account. The proposed phase synchrony methods could be extended to measure the directionality of the phase synchrony either by using the directionality index proposed by Rosenblum and Pikovsky [46] or by computing the phase synchrony measures using time-shifted signals.

6.2.4 Functional Networks

The proposed phase synchrony measures can be extended to determine the functional network patterns in the brain across space, time, and frequency. The measures will be the first step in defining adjacency matrices which can be used in graph theoretic analysis of functional networks to determine the organization patterns of the brain such as small world network models. Furthermore, if a directional measure is used, a directional network could be created. Once a network is constructed, methods in graph theory could be applied for analysis. Stam et al. converted synchronization matrices similar to the ones seen in Figures 5.1 and 5.2 into graphs and applied methods from graph theory such as the clustering coefficient and path length[47].

BIBLIOGRAPHY

BIBLIOGRAPHY

- [1] R.S.J. Frackowiak, K. Friston, C. Frith, R. Dolan, C.J. Price, S. Zeki, J. Ashburner, and W. Penny, *Human Brain Function*, Academic Press, 2003.
- [2] O. David, D. Cosmelli, J.P. Lachaux, S. Baillet, L. Garnero, and J. Martinerie, "A theoretical and experimental introduction to the non-invasive study of large-scale neural phase synchronization in human beings," *International Journal of Computational Cognition*, vol. 1, pp. 53–77, 2002.
- [3] E. Rodriguez, N. George, J.P. Lachaux, J. Martinerie, B. Renault, and F.J. Varela, "Perception's shadow: long-distance synchronization of human brain activity," *Nature*, vol. 397, no. 6718, pp. 430–433, 1999.
- [4] D. Rudrauf, A. Douiri, C. Kovach, J.P. Lachaux, D. Cosmelli, M. Chavez, C. Adam, B. Renault, J. Martinerie, and M. Le Van Quyen, "Frequency flows and the time-frequency dynamics of multivariate phase synchronization in brain signals," *Neuroimage*, vol. 31, no. 1, pp. 209–227, 2006.
- [5] E. Başar, EEG-Brain Dynamics: Relation Between EEG and Brain Evoked Potentials, Elsevier-North-Holland Biomedical Press, 1980.
- [6] B.J. Fisch, Fisch and Spehlmann's EEEG Primer: Basic Principles of Digital and Analog EEG, Elsevier Science Health Science, 1999.
- [7] G. Tononi, G.M. Edelman, and O. Sporns, "Complexity and coherency: integrating information in the brain," *Trends in Cognitive Sciences*, vol. 2, no. 12, pp. 474–484, 1998.
- [8] F. Varela, J.P. Lachaux, E. Rodriguez, and J. Martinerie, "The brainweb: phase synchronization and large-scale integration," *Nature Reviews Neuroscience*, vol. 2, no. 4, pp. 229–239, 2001.
- [9] A. Von Stein, P. Rappelsberger, J. Sarnthein, and H. Petsche, "Synchronization between temporal and parietal cortex during multimodal object processing in man," *Cerebral Cortex*, vol. 9, no. 2, pp. 137–150, 1999.
- [10] V. Samar, K. Swartz, and M. Raghuveer, "Multiresolution analysis of event-related potentials by wavelet decomposition," *Brain and Cognition*, vol. 27, no. 3, pp. 398–438, 1995.
- [11] J. Raz, L. Dickerson, and B. Turetsky, "A wavelet packet model of evoked potentials," *Brain and Language*, vol. 66, no. 1, pp. 61–88, 1999.
- [12] R. Quiroga, O.W. Sakowitz, E. Basar, and M. Schürmann, "Wavelet trans-

- form in the analysis of the frequency composition of evoked potentials," *Brain Research Protocols*, vol. 8, no. 1, pp. 16–24, 2001.
- [13] P. Zarjam, G. Azemi, M. Mesbah, and B. Boashash, "Detection of newborns' EEG seizure using time-frequency divergence measures," in *Proceedings of the IEEE International Conference of Acoustics, Speech and Signal Processing*, 2004, vol. 5, pp. 429–432.
- [14] M. Sun, M.L. Scheuer, S. Qian, S.B. Baumann, P.D. Adelson, and R.J. Sclabassi, "Time-frequency analysis of high-frequency activity at the start of epileptic seizures," in *Proceedings of the IEEE International Conference on Engineering in Medicine and Biology*, 1997, vol. 3, pp. 1184–1187.
- [15] M. Carlos Guerrero, A.M. Trigueros, and J.I. Franco, "Time-frequency EEG analysis in epilepsy: What is more suitable?," in *Proceedings of the IEEE International Symposium on Signal Processing and Information Technology*, 2005, pp. 202–207.
- [16] P. Zarjam and M. Mesbah, "Discrete wavelet transform based seizure detection in newborns EEG signals," in *Proceedings of the Seventh International Symposium on Signal Processing and Its Applications*, 2003, vol. 2, pp. 459–462.
- [17] P. Zarjam, M. Mesbah, and B. Boashash, "Detection of newborn EEG seizure using optimal features based on discrete wavelet transform," in *Proceedings of the IEEE International Conference on Acoustics, Speech and Signal Processing*, 2003, vol. 2, pp. 265–268.
- [18] R. Polikar, M.H. Greer, L. Udpa, and F. Keinert, "Multiresolution wavelet analysis of ERPs for the detection of Alzheimer's disease," in *Proceedings of the IEEE 19th International Conference of Engineering in Medicine and Biology Society*, 1997, pp. 1301–1304.
- [19] G. Jacques, J.L. Frymiare, J. Kounios, C. Clark, and R. Polikar, "Multiresolution analysis for early diagnosis of Alzheimer's disease," in *Proceedings of 26th Annual International Conference of IEEE Engineering in Medicine and Biology Society*, 2004, vol. 1, pp. 251–254.
- [20] K.M. Spencer, P.G. Nestor, M.A. Niznikiewicz, D.F. Salisbury, M.E. Shenton, and R.W. McCarley, "Abnormal neural synchrony in schizophrenia," *Journal of Neuroscience*, vol. 23, no. 19, pp. 7407–7411, 2003.
- [21] N. Hazarika, J.Z. Chen, A.C. Tsoi, and A. Sergejew, "Classification of EEG signals using the wavelet transform," *Signal Processing*, vol. 59, no. 1, pp. 61–72, 1997.
- [22] L. Cohen, Time-frequency analysis: theory and applications, Prentice Hall,

1995.

- [23] A. Rihaczek, "Signal energy distribution in time and frequency," *IEEE Transactions on Information Theory*, vol. 14, no. 3, pp. 369–374, 1968.
- [24] J.P. Lachaux, A. Lutz, D. Rudrauf, D. Cosmelli, M. Le Van Quyen, J. Martinerie, and F. Varela, "Estimating the time-course of coherence between single-trial brain signals: an introduction to wavelet coherence," *Neurophysiologie Clinique/Clinical Neurophysiology*, vol. 32, no. 3, pp. 157–174, 2002.
- [25] A. Ambardar, Analog and digital signal processing, PWS, 2002.
- [26] S. Haykin, R.J. Racine, Y. Xu, and C.A. Chapman, "Monitoring neuronal oscillations and signal transmission between cortical regions using time-frequency analysis of electroencephalographic activity," *Proceedings of the IEEE*, vol. 84, no. 9, pp. 1295–1301, 1996.
- [27] M. Le Van Quyen, J. Foucher, J.P. Lachaux, E. Rodriguez, A. Lutz, J. Martinerie, and F.J. Varela, "Comparison of Hilbert transform and wavelet methods for the analysis of neuronal synchrony," *Journal of Neuroscience Methods*, vol. 111, no. 2, pp. 83–98, 2001.
- [28] J.P. Lachaux, E. Rodriguez, M. Le Van Quyen, A. Lutz, J. Martinerie, and F.J. Varela, "Studying single-trials of phase synchronous activity in the brain," *International Journal of Bifurcation and Chaos*, vol. 10, pp. 2429–2439, 2000.
- [29] D. Li and R. Jung, "Quantifying coevolution of nonstationary biomedical signals using time-varying phase spectra," *Annals of Biomedical Engineering*, vol. 28, no. 9, pp. 1101–1115, 2000.
- [30] S. Aviyente, W.S. Evans, E.M. Bernat, and S. Sponheim, "A time-varying phase coherence measure for quantifying functional integration in the brain," in *Proceedings of the IEEE International Conference on Acoustics, Speech and Signal Processing*, 2007, vol. 4, pp. 1169–1172.
- [31] J.P. Lachaux, E. Rodriguez, J. Martinerie, and F.J. Varela, "Measuring phase synchrony in brain signals," *Human Brain Mapping*, vol. 8, pp. 194–208, 1999.
- [32] C. Allefeld and J. Kurths, "An approach to multivariate phase synchronization analysis and its application to event-related potentials," *International Journal of Bifurcation and Chaos*, vol. 14, no. 2, pp. 417–426, 2004.
- [33] C. Allefeld and J. Kurths, "Multivariate phase synchronization analysis of EEG data," *IEICE Transactions on Fundamentals of Electronics, Communications, and Computer Sciences*, vol. 86, no. 9, pp. 2218–2221, 2003.
- [34] B. Boashash, "Estimating and interpreting the instantaneous frequency of a

- signal-part 2: algorithms and applications," *Proceedings of the IEEE*, vol. 80, no. 4, pp. 540-568, 1992.
- [35] L. Rankine, M. Mesbah, and B. Boashash, "IF estimation for multicomponent signals using image processing techniques in the time-frequency domain," *Signal Processing*, vol. 87, no. 6, pp. 1234–1250, 2007.
- [36] K.J. Friston, "Schizophrenia and the disconnection hypothesis," *Acta Psychiatrica Scandinavica*, vol. 99, pp. 68–79, 1999.
- [37] L.D. Selemon and P.S. Goldman-Rakic, "The reduced neuropil hypothesis: a circuit based model of schizophrenia," *Biological Psychiatry*, vol. 45, no. 1, pp. 17–25, 1999.
- [38] F.M. Benes, "Emerging principles of altered neural circuitry in schizophrenia," *Brain Research Reviews*, vol. 31, no. 2-3, pp. 251–269, 2000.
- [39] G. Tononi and G.M. Edelman, "Schizophrenia and the mechanisms of conscious integration," *Brain Research Reviews*, vol. 31, no. 2-3, pp. 391–400, 2000.
- [40] P. Fries, S. Neuenschwander, A.K. Engel, R. Goebel, and W. Singer, "Rapid feature selective neuronal synchronization through correlated latency shifting," *Nature Neuroscience*, vol. 4, pp. 194–200, 2001.
- [41] J.S. Kwon, B.F. O'Donnell, G.V. Wallenstein, R.W. Greene, Y. Hirayasu, P.G. Nestor, M.E. Hasselmo, G.F. Potts, M.E. Shenton, and R.W. McCarley, "Gamma frequency-range abnormalities to auditory stimulation in schizophrenia," *Archives of General Psychiatry*, vol. 56, no. 11, pp. 1001–1005, 1999.
- [42] P.J. Uhlhaas, D.E.J. Linden, W. Singer, C. Haenschel, M. Lindner, K. Maurer, and E. Rodriguez, "Dysfunctional long-range coordination of neural activity during gestalt perception in schizophrenia," *Journal of Neuroscience*, vol. 26, no. 31, pp. 8168–8175, 2006.
- [43] F. Perrin, O. Bertrand, and J. Pernier, "Scalp Current Density Mapping: Value and Estimation from Potential Data," *IEEE Transactions on Biomedical Engineering*, pp. 283–288, 1987.
- [44] J. Le and A. Gevins, "Method to reduce blur distortion from EEG's using a realistic headmodel," *IEEE Transactions on Biomedical Engineering*, vol. 40, no. 6, pp. 517–528, 1993.
- [45] E. Pereda, R.Q. Quiroga, and J. Bhattacharya, "Nonlinear multivariate analysis of neurophysiological signals," *Progress in Neurobiology*, vol. 77, no. 1-2, pp. 1-37, 2005.

- [46] M.G. Rosenblum and A.S. Pikovsky, "Detecting direction of coupling in interacting oscillators," *Physical Review E*, vol. 64, no. 4, pp. 45202, 2001.
- [47] C.J. Stam, B.F. Jones, G. Nolte, M. Breakspear, and P. Scheltens, "Smallworld networks and functional connectivity in alzheimer's disease," *Cerebral Cortex*, vol. 17, no. 1, pp. 92–99, 2007.

